AGU PUBLICATIONS

JGR

Journal of Geophysical Research: Biogeosciences

RESEARCH ARTICLE
10.1002/2015JG003052

Key Points:
- Photochemical degradability of western Arctic Ocean DOM was tested in a solar simulator
- Solar irradiation caused significant decreases in CDOM light absorption at UV wavelengths
- Continued declines in sea ice cover should result in enhanced CDOM photodegradation

Correspondence to:
K. E. Frey,
kfrey@clarku.edu

Citation:
Logvinova, C. L., K. E. Frey, P. J. Mann, A. Stubbins, and R. G. M. Spencer (2015), Assessing the potential impacts of declining Arctic sea ice cover on the photochemical degradation of dissolved organic matter in the Chukchi and Beaufort Seas, *J. Geophys. Res. Biogeosci.*, *120*, 2326–2344, doi:10.1002/2015JG003052.

Received 8 MAY 2015
Accepted 23 OCT 2015
Accepted article online 29 OCT 2015
Published online 23 NOV 2015

Assessing the potential impacts of declining Arctic sea ice cover on the photochemical degradation of dissolved organic matter in the Chukchi and Beaufort Seas

Christie L. Logvinova[1], Karen E. Frey[1], Paul J. Mann[2], Aron Stubbins[3], and Robert G. M. Spencer[4]

[1]Graduate School of Geography, Clark University, Worcester, Massachusetts, USA, [2]Department of Geography, Northumbria University, Newcastle upon Tyne, UK, [3]Skidaway Institute of Oceanography, Department of Marine Science, University of Georgia, Savannah, Georgia, USA, [4]Department of Earth, Ocean and Atmospheric Science, Florida State University, Tallahassee, Florida, USA

Abstract A warming and shifting climate in the Arctic has led to significant declines in sea ice over the last several decades. Although these changes in sea ice cover are well documented, large uncertainties remain in how associated increases in solar radiation transmitted to the underlying ocean water column will impact heating, biological, and biogeochemical processes in the Arctic Ocean. In this study, six under-ice marine, two ice-free marine, and two ice-free terrestrially influenced water samples were irradiated using a solar simulator for 72 h (representing ~10 days of ambient sunlight) to investigate dissolved organic matter (DOM) dynamics from the Chukchi and Beaufort Seas. Solar irradiation caused chromophoric DOM (CDOM) light absorption at 254 nm to decrease by 48 to 63%. An overall loss in total DOM fluorescence intensity was also observed at the end of all experiments, and each of six components identified by parallel factor (PARAFAC) analysis was shown to be photoreactive in at least one experiment. Fluorescent DOM (FDOM) also indicated that the majority of DOM in under-ice and ice-free marine waters was likely algal-derived. Measurable changes in dissolved organic carbon (DOC) were only observed for sites influenced by riverine runoff. Losses of CDOM absorbance at shorter wavelengths suggest that the beneficial UV protection currently received by marine organisms may decline with the increased light transmittance associated with sea ice melt ponding and overall reductions of sea ice. Our FDOM analyses demonstrate that DOM irrespective of source was susceptible to photobleaching. Additionally, our findings suggest that photodegradation of CDOM in under-ice waters is not currently a significant source of carbon dioxide (CO_2) (i.e., we did not observe systematic DOC loss). However, increases in primary production and terrestrial freshwater export expected under future climate change scenarios may cause an increase in CDOM quantity and shift in quality throughout Arctic Ocean surface waters. As Arctic temperatures continue to warm and summer sea ice further declines, examination of the resulting enhanced photodegradation processes and their impacts on the interplay between primary production, carbon cycling, and surface ocean heating processes will be paramount.

1. Introduction

Recent climate warming has caused significant decreases in sea ice extent across the Arctic [*Serreze et al.*, 2007; *Stroeve et al.*, 2007; *Comiso et al.*, 2008], with a record minimum in September 2012 that was 49% below the 1979–2000 average [*Perovich et al.*, 2012]. Over the past three decades, there has also been an increase in the length of the summer melt season [*Markus et al.*, 2009] and an increasing percentage of thin first-year ice as compared with thicker multiyear ice [*Maslanik et al.*, 2007; *Kwok and Rothrock*, 2009; *Maslanik et al.*, 2011; *Comiso*, 2012]. Declining sea ice extent reduces surface albedo, thereby enhancing the amount of solar radiation absorbed by associated ocean waters and ice. Furthermore, melt ponds form more easily and cover more surface area on thin first-year ice than on multiyear ice [*Fetterer and Untersteiner*, 1998; *Nicolaus et al.*, 2012], and light transmittance through these melt ponds can be up to an order of magnitude greater than through unponded sea ice [*Light et al.*, 2008; *Frey et al.*, 2011; *Nicolaus et al.*, 2012]. In future climate scenarios, Arctic sea ice is expected to continue thinning, decreasing in areal extent, and increasing its melt pond coverage [*Wang and Overland*, 2009; *Schröder et al.*, 2014], yet large uncertainties remain in how the resulting increase in solar radiation transmitted to the underlying ocean waters will impact biological and biogeochemical processes in the Arctic Ocean.

A major uncertainty linked to sea ice decline is to what extent dissolved organic matter (DOM) in underlying ocean waters will be impacted. In the Arctic Ocean, DOM primarily results from either (a) in situ biological

production in the upper water column and within sea ice or (b) inputs of terrestrially derived organic matter transported to the ocean by fluvial systems [*Carlson*, 2002; *Holmes et al.*, 2012; *Raymond and Spencer*, 2015]. Chromophoric DOM (CDOM) is the optically active fraction of this dissolved material, absorbing ultraviolet (UV) and visible light, and acting as one of the primary regulators of light penetration in surface waters [*Blough and Del Vecchio*, 2002; *Nelson and Siegel*, 2002]. CDOM regulates the amount of photosynthetically active radiation (PAR) in the water column, which influences the rates and distribution patterns of primary production [*Retamal et al.*, 2008]. CDOM also efficiently blocks UV radiation, thereby protecting marine organisms from DNA damage and other harmful effects [*Williamson et al.*, 2001]. By absorbing shortwave visible radiation (380–760 nm), CDOM can additionally contribute to the heating of surface waters and subsequent melting of sea ice [*Kirk*, 1988, 1994; *Pegau*, 2002; *Granskog et al.*, 2007; *Hill*, 2008]. The absorption of light by CDOM can lead to photodegradation of DOM [*Mopper et al.*, 2015], generally resulting in a decrease in CDOM absorption (i.e., photobleaching) [*Helms et al.*, 2008, 2014]. Through these photodegradation processes, a pool of DOM can be directly photomineralized to inorganic carbon, with subsequent outgassing of CO_2 to the atmosphere [*Stubbins et al.*, 2008; *Powers and Miller*, 2015]. In addition, photochemical alteration of DOM influences the bioavailability of residual DOM to aquatic bacteria [*Moran and Zepp*, 1997; *Bittar et al.*, 2015]. The presence and characteristics of Arctic sea ice can therefore play a critical role in determining light penetration, in turn influencing CDOM distribution and biogeochemical cycling in surface ocean waters.

Over the past ~30 years, the Chukchi and Beaufort Seas of the western Arctic have experienced some of the greatest declines in sea ice extent across the Arctic Ocean [*Comiso et al.*, 2008], exposing the marine environment in this region to continually increasing amounts of solar radiation [*Perovich et al.*, 2007]. To date, only a few studies have investigated DOM in the western Arctic Ocean, with these typically focusing on the distribution of CDOM in open waters [*Gueguen et al.*, 2005, 2007; *Retamal et al.*, 2007; *Matsuoka et al.*, 2007, 2011; *Hill*, 2008; *Walker et al.*, 2009]. Furthermore, given the heavily riverine-influenced nature of the Arctic Ocean [*Opsahl et al.*, 1999; *Dittmar and Kattner*, 2003], DOM photoreactivity studies have focused primarily on terrigenous DOM in the coastal regions [*Belanger et al.*, 2006; *Osburn et al.*, 2009]. Thus, despite the critical need to understand the impacts of a shrinking and thinning sea ice cover, to the best of our knowledge this work represents the first study to focus upon the photoreactivity of DOM beneath sea ice. In this study, we used a series of controlled laboratory-based photodegradation experiments to investigate DOM dynamics in under-ice ocean waters collected from the Chukchi and Beaufort Seas during the summer of 2011. Absorbance and fluorescence spectroscopy were used to identify the likely source of DOM and to trace changes in CDOM optical properties during photochemical degradation. These results were then examined alongside changes in dissolved organic carbon (DOC) concentration to assess the relative importance of photobleaching and photomineralization. Finally, we discuss the potential photochemical susceptibility of Arctic Ocean DOM and how future changes to sea ice may influence primary productivity, carbon biogeochemistry, and the heat balance in the Arctic Ocean.

2. Methods

2.1. Sample Collection

Sampling took place during the NASA Impacts of Climate Change on the Eco-Systems and Chemistry of the Arctic Pacific Environment (ICESCAPE) mission in the Chukchi and Beaufort Seas during the summer melt season in July 2011 on the U.S. Coast Guard Cutter (USCGC) *Healy*. Water samples were collected from 10 locations distributed across three north-south transects (Figure 1), including samples from ice-free marine (IFM), ice-covered marine (ICM), and ice-free terrestrially influenced (IFT) locations. The westernmost transect was located on the continental shelf of the Chukchi Sea (IFM_1 and ICM_{1-3}). The central transect crossed the shelf-basin interface in the Chukchi Sea (IFM_2 and ICM_{4-5}). The easternmost transect extended into a region of the Beaufort Sea basin impacted by river runoff, primarily from the Colville River (IFT_{1-2} and ICM_6).

At six ice-covered stations (ICM_{1-6}; Figure 1), water samples were collected from directly below the ice at the ice-water interface by hand-deploying a 2 L Kemmerer (vertically oriented) water sampler. At the remaining four stations located in open water, surface water samples were collected using the ship's conductivity-temperature-depth rosette, which consisted of a 12-place rosette with 30 L Niskin bottles. Two of these stations were located near the ice edge (IFM_{1-2}; Figure 1), and two were from surface waters likely influenced by the Colville River (IFT_{1-2}). Salinity measurements for each sample were made on board using a Guildline

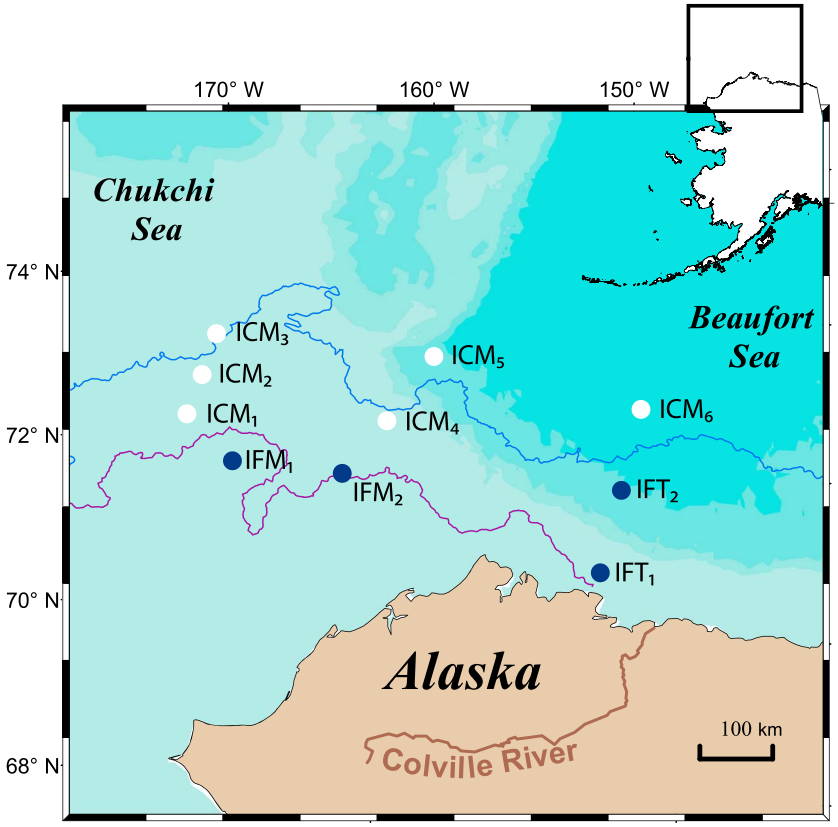

Figure 1. Station locations for under-ice marine samples (white), ice-free marine samples (blue), and terrestrially influenced samples (blue). The location of the ice edge on the first day of sampling (3 July 2011) and the last day of sampling (21 July 2011) are indicated by the purple and blue lines, respectively.

Autosal salinometer. Immediately after sampling, water samples for photodegradation experiments were filtered through a prerinsed 0.2 μm filter (Whatman Polycap) and transferred into acid-washed (10% HCl) precombusted (450°C for 6 h) Kimax glass bottles. Samples were kept frozen (−20°C) and dark until return to the laboratory.

2.2. Photodegradation Experiments

After slowly thawing overnight, water samples were transferred into acid-washed (10% HCl), precombusted (450°C for 6 h) round bottom quartz flasks (70 mL; Quartz Scientific Inc., OH, USA) and closed with ground-glass stoppers to exclude air bubbles. Flasks were rinsed with sample water 3 times prior to filling and then placed bottomside up in a 20°C water bath containing Milli-Q water. Samples were positioned just under the water surface. The bath was mounted inside an Atlas SUNTEST XLS+ solar simulator fitted with an Atlas NXe 1700 W bulb and daylight filter, to provide a light spectrum similar to that of natural sunlight between 280 and 800 nm. Total lamp power was 765 W m^{-2} with a constant exposure of 65 W m^{-2} between 300 to 400 nm. Samples were exposed for 72 h, receiving a radiant exposure of 16,865 ± 6.7 kJ m^{-2} of energy (time integral of spectral irradiance), equivalent to approximately 10 days of ambient sunlight during the summer months at 70°N (based on the System for Transfer of Atmospheric Radiation [*Ruggaber et al.*, 1994] and following adaptations described in *Powers and Miller* [2015]). CDOM, fluorescent DOM (FDOM), and DOC were measured (details below) at the beginning of the experiment and then again after 4, 12, 24, and 72 h of light exposure. Triplicate samples and a single dark control (treated identically but wrapped in foil) were used at all time points, with triplicate dark controls for the initial and final (72 h) time points.

2.3. CDOM Analysis

CDOM absorbance was measured using a Shimadzu UV-1800 UV-Visible spectrophotometer at 1 nm intervals between 800 and 200 nm using a 10 cm quartz cuvette. All sample spectra were blank corrected and

referenced against Milli-Q water (18.2 Ω). In order to minimize temperature effects, all measurements were made after samples had equilibrated to laboratory temperature. CDOM absorbance was assumed to be zero above 750 nm; therefore, the average sample absorbance between 750 nm and 800 nm was subtracted from the spectrum to correct for offsets owing to instrument baseline drift, temperature, scattering, and refractive effects [*Green and Blough*, 1994; *Helms et al.*, 2008]. CDOM absorption coefficients were calculated from

$$\alpha(\lambda) = 2.303A(\lambda)/l \quad (1)$$

where a is the Naperian light absorption coefficient (m^{-1}) at λ (the wavelength in nanometers), A is the absorbance at λ wavelength, and l is the cell path length in meters [*Green and Blough*, 1994].

Spectral slopes (S, nm^{-1}) for each CDOM absorbance spectrum were derived using an exponential function:

$$\alpha(\lambda) = \alpha(\lambda_0)e^{-S(\lambda-\lambda_0)} \quad (2)$$

where a (λ) is the absorption coefficient of CDOM (m^{-1}) at wavelength λ and λ_0 is the reference wavelength. Spectral slopes were calculated across the wavelength ranges of 275–295 nm and 350–400 nm. Spectral slope parameters can provide information pertaining to DOM molecular weight, photochemical processing, and source [*Blough and Del Vecchio*, 2002; *Helms et al.*, 2008] and have been found to be largely independent of CDOM concentration [*Brown*, 1977]. The 275–295 nm and 350–400 nm slope ranges were chosen as they have been shown to contain the greatest variation in a wide range of samples, including DOM-rich terrestrial, estuarine, coastal, and highly photobleached waters [*Helms et al.*, 2008; *Spencer et al.*, 2012]. The ratio of these slopes (S_R) has been shown to be particularly sensitive to changes in molecular weight and was calculated by dividing $S_{275–295}$ by $S_{350–400}$ [*Helms et al.*, 2008]. All slopes are reported as positive numbers, such that higher (i.e., steeper) slopes indicate a greater decrease in absorption with increasing wavelength.

2.4. FDOM Analysis

The fluorescent portion of CDOM (FDOM) was characterized using fluorescence excitation emission matrix (EEM) spectroscopy, which creates three-dimensional structures composed of multiple emission spectra at a range of excitations and provides additional information about the chemical composition and sources of CDOM [*Coble*, 1996, 2007; *Stedmon et al.*, 2003; *Stubbins et al.*, 2014]. FDOM measurements were collected on a FluoroMax 4 spectrofluorometer (Horiba Jobin-Yvon). EEMs were obtained by recording sample emission across 320 to 500 nm (with 2 nm increments) after excitation from 250 to 450 nm wavelengths (with 5 nm increments). A single sample EEM was collected at each time point (0, 4, 12, 24, and 72 h). Owing to low fluorescence intensities, samples were run using long integration periods (0.5 s) to minimize measurement noise. All EEMs were blank corrected and Raman calibrated [*Lawaetz and Stedmon*, 2009; *Murphy et al.*, 2010] using Milli-Q water spectra run on the same day. Finally, to eliminate Rayleigh scattering effects, zeroes were inserted in the region where emission wavelengths are less than or equal to the excitation wavelength (+30 nm). The absorption coefficients of all samples were $<10\ m^{-1}$, eliminating the need for inner filter corrections [*Stedmon and Bro*, 2008; *Murphy et al.*, 2010].

Many fluorescent components have overlapping peaks making it difficult to identify individual components within an EEM. To identify independently varying FDOM components within our data set, and to assess changes in marine versus Terrestrially derived material, we conducted parallel factor (PARAFAC) analysis in MATLAB using the DOMFluor Toolbox following the methods as outlined in *Stedmon and Bro* [2008]. In total, we included 50 EEMs containing five different time points for each of the 10 experiments. By tracing processes using time series measurements of FDOM, PARAFAC modeling may yield more meaningful results than if applied to discrete samples [*Stedmon and Bro*, 2008]. To simplify the modeling process and minimize noise, we included only emission wavelengths from 320 to 476 nm in the EEMs. No EEMs were identified as outliers. A series of PARAFAC models (utilizing between two to seven components) were applied and initial model fitting assessed using the steps as outlined in *Stedmon and Bro* [2008]. Final model validation was conducted using a range of techniques including random split half analysis and random initialization [*Stedmon and Bro*, 2008]. Split half validation involves splitting the sample data into two halves and comparing model fits after running models on the two halves independently. Random initialization was then used to ensure that the models were in fact the least squares result and represented local minima.

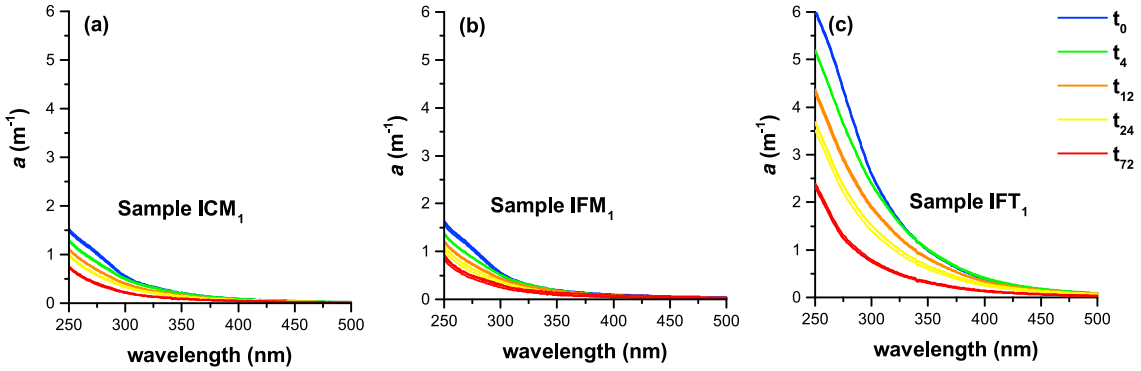

Figure 2. Loss of CDOM absorbance with irradiation for triplicate samples from experiments (a) ICM_1, (b) IFM_1, and (c) IFT_1. CDOM absorbance is shown at the start of the experiment (t_0) and after 4, 12, 24, and 72 h (t_4, t_{12}, t_{24}, and t_{72}).

2.5. Dissolved Organic Carbon Analysis

After the experiments, samples for DOC analyses were acidified (pH < 2) by addition of HCl and analyzed for nonpurgable organic carbon using a Shimadzu TOC-VCPH analyzer fitted with a Shimadzu ASI-V autosampler. Standards were prepared by the volumetric dilution of a stock solution containing 500 μM DOC (potassium hydrogen phthalate, analytical grade) to produce the following series of standards: 0, 2, 5, 8, 10, 25, 50, 75,

Table 1. Initial, Final, and Percent Remaining After 72 h Irradiation Experiments for a_{254} and DOC for All Experiments[a]

Sample Name	Collection Date	Salinity		a_{254} (m^{-1})	DOC (μM)
ICM_1	7/4/2011	17.4	Initial	1.41 ± 0.03	67.8 ± 0.8
			Final	0.66 ± 0.02	65.8 ± 1.2
			% Remaining	**47.1**	97.0
ICM_2	7/5/2011	30.7	Initial	1.55 ± 0.01	71.9 ± 2.8
			Final	0.72 ± 0.02	68.7 ± 1.2
			% Remaining	**46.5**	95.6
ICM_3	7/6/2011	29.7	Initial	1.37 ± 0.04	61.1 ± 2.5
			Final	0.62 ± 0.01	60.6 ± 0.4
			% Remaining	**44.8**	99.1
ICM_4	7/10/2011	22.4	Initial	1.36 ± 0.02	53.6 ± 3.9
			Final	0.63 ± 0.01	53.7 ± 2.4
			% Remaining	**46.5**	100.2
ICM_5	7/13/2011	24.9	Initial	2.17 ± 0.01	71.1 ± 0.1
			Final	0.98 ± 0.03	68.0 ± 1.3
			% Remaining	**44.9**	95.6
ICM_6	07/19/11	20.8	Initial	2.01 ± 0.03	69.4 ± 0.6
			Final	0.98 ± 0.02	67.0 ± 0.8
			% Remaining	**48.7**	**96.6**
IFM_1	7/3/2011	31.7	Initial	1.49 ± 0.04	
			Final	0.77 ± 0.04	*NA*
			% Remaining	**51.8**	
IFM_2	7/9/2011	31.1	Initial	1.89 ± 0.01	71.2 ± 0.9
			Final	0.83 ± 0.02	71.9 ± 1.1
			% Remaining	**44.0**	100.9
IFT_1	07/21/11	28.0	Initial	5.79 ± 0.03	105.4 ± 1.4
			Final	2.17 ± 0.05	97.1 ± 2.5
			% Remaining	**37.4**	**92.1**
IFT_2	07/20/11	24.4	Initial	3.12 ± 0.00	80.5 ± 1.2
			Final	1.48 ± 0.06	74.7 ± 0.6
			% Remaining	**47.4**	**92.8**

[a]Bold numbers indicate statistically significant changes ($p < 0.05$). *NA* indicates that the value is unavailable owing to sample loss.

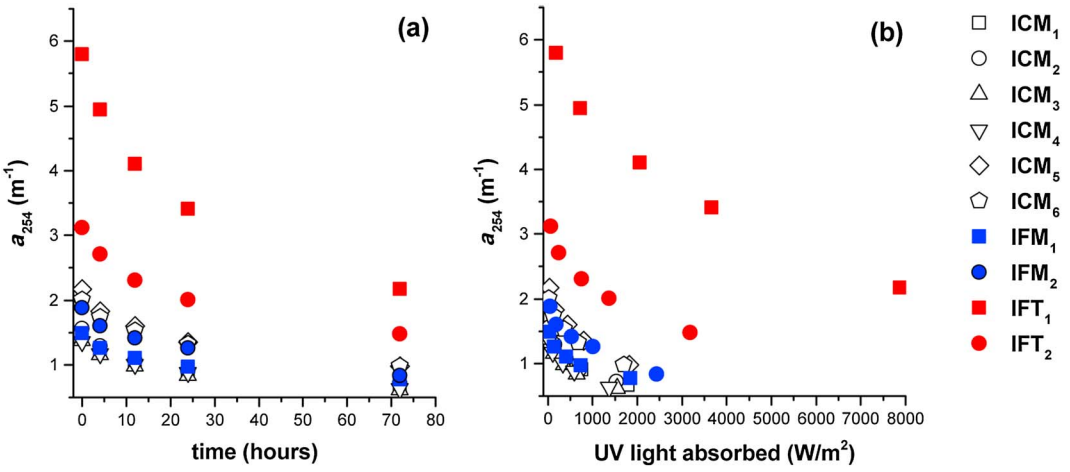

Figure 3. Loss of CDOM absorbance at 254 nm as a function of (a) time and (b) the amount of cumulative UV light (280–400 nm) absorption at each time interval for all experiments.

and 100 μM DOC. In addition to standards, aliquots of deep seawater reference material (Batch 10, Lot# 05–10) from the Consensus Reference Material (CRM) project were analyzed to ensure the precision and accuracy of the DOC analyses. Analyses of the CRM deviated by less than 5% from the reported value for these standards (41 to 44 μM DOC; http://yyy.rsmas.miami.edu/groups/biogeochem/Table1.htm). Standard and sample volumes analyzed were 20 to 40 mL. Routine minimum detection limits in the investigators laboratory using the above configuration are 2.8 ± 0.3 μM C, and standard errors are typically 1.7 ± 0.5% of the DOC concentration [*Stubbins and Dittmar*, 2012].

3. Results

3.1. Photodegradation of CDOM

Photodegradation experiments were conducted on waters from 10 separate stations across the Chukchi and Beaufort Seas. Figure 2 shows absorption coefficient spectra over the course of a 72 h experiment (including triplicate analyses for each time step) for a typical ice-covered marine (ICM_1), ice-free marine (IFM_1), and ice-free terrestrially influenced (IFT_1) sample. CDOM measurements from replicate samples at each individual time step and experiment demonstrated little between-flask variability (with a coefficient of variance <0.06 at 254 nm for all experiments). Therefore, from here on we present only sample means of triplicate measurements. All under-ice (ICM_{1-6}) and ice-free marine samples (IFM_{1-2}) had lower initial CDOM absorption values (ranging from 1.36 to 2.17 m^{-1} at 254 nm) than terrestrially influenced (IFT_{1-2}) samples (3.12 to 5.79 m^{-1} at 254 nm). Despite these initial differences, CDOM from all 10 stations was found to be photoreactive (Table 1 and Figure 3a). For all experiments, photochemically induced changes in the absorption coefficient at 254 nm (a_{254}) over the 72 h period were found to be statistically significant ($p < 0.05$; two-tailed Student's *t* test on triplicate samples from the beginning and end of each experiment) with total losses in a_{254} of between 48 and 63%. No significant differences were observed between initial a_{254} values and those of the dark controls after 72 h ($p < 0.05$) across any of the experiments, confirming photochemical processes that led to the observed reductions in absorbance. With the exception of samples ICM_5 and IFM_1, sample waters also showed

Table 2. Average Initial and Final Values for the 72 h Irradiation Experiments for a_{254}, a_{365}, and a_{440} for Ice-Covered Marine (ICM), Ice-Free Marine (IFM), and Ice-Free Terrestrial (IFT) Samples

		a_{254} (m^{-1})	a_{365} (m^{-1})	a_{440} (m^{-1})
ICM_{mean}	Initial	1.62 ± 0.32	0.14 ± 0.02	0.04 ± 0.01
	Final	0.76 ± 0.16	0.06 ± 0.01	0.02 ± 0.01
IFM_{mean}	Initial	1.69 ± 0.22	0.17 ± 0.03	0.06 ± 0.01
	Final	0.80 ± 0.05	0.08 ± 0.02	0.04 ± 0.01
IFT_{mean}	Initial	4.46 ± 1.46	0.50 ± 0.29	0.13 ± 0.08
	Final	1.82 ± 0.38	0.18 ± 0.08	0.05 ± 0.03

Table 3. Three-Parameter Exponential Decay Models for a_{254} Versus Cumulative UV Light Absorbed for All Experiments

	ICM_1	ICM_2	ICM_3	ICM_4	ICM_5	ICM_6	IFM_1	IFM_2	IFT_1	IFT_2
z_0	0.78	0.90	0.80	0.80	1.28	1.08	0.73	1.17	4.21	1.77
K	1.64	2.25	1.94	1.74	1.41	1.54	1.96	0.82	0.25	0.81
C_∞	0.63	0.71	0.59	0.57	0.89	0.91	0.76	0.68	1.63	1.36
C (0)	1.42	1.60	1.39	1.36	2.17	1.99	1.49	1.86	5.84	3.13
R^2	0.96	0.98	0.97	0.97	0.96	0.96	0.96	0.94	0.98	0.98

statistically significant photobleaching at 365 nm (a_{365}), with a greater decrease observed in the IFT samples than in the marine samples (Table 2). Initial absorption coefficients at 440 nm (a_{440}) were relatively low (most were at or below the detection limit of the spectrophotometer (±0.002 absorbance or 0.05 m^{-1})), and losses in a_{440} were not statistically significant for 7 of the 10 experiments (Table 2).

CDOM absorption values at 254 nm for the marine samples, whether from under-ice (ICM) or ice-free (IFM) waters, were not significantly different from one another (at both initial and final time points), yet both were statistically different ($p < 0.05$) from terrestrially influenced samples. Overall, the marine samples had lower initial a_{254} values (mean for ICM and IFM = 1.65 m^{-1}) and exhibited smaller decreases in a_{254} (mean = 0.88 m^{-1}) as compared to the terrestrially influenced samples (mean a_{254} = 4.46 m^{-1}, showing a mean loss of 2.63 m^{-1}; Table 2).

As samples were not all optically thin, to more accurately determine changes in the efficiency of photobleaching between samples, the CDOM absorption coefficient was additionally plotted as a function of cumulative UV light (280–400 nm) absorbed (Figure 3b). The range of 280–400 nm was chosen because these are quantitatively the most important wavelengths for environmental photoreactions involving CDOM [*Mopper et al.*, 2015]. The decrease in the CDOM absorption coefficient at 254 nm was approximately exponential and could be modeled using the following three-parameter exponential decay equation:

$$C(u) = C_\infty + z_0 e^{-ku} \tag{3}$$

where u is the cumulative UV light absorbed in kW/m^2, $C(u)$ is the modeled absorption coefficient, C_∞ is the nonphotoreactive component, z_0 is the photoreactive component, and k is the rate of decay. The exponential decay models fit the experimental results well with adjusted R^2 values ranging from ~0.94 to 0.98 for all experiments (Table 3). Overall, marine samples had smaller photoreactive components (z_0) and residual nonphotoreactive (C_∞) components compared to the terrestrially influenced samples. Additionally, the rate of decay (k) was greater for marine samples compared to the terrestrially influenced samples, with the exception of IFM_2 which had a rate of decay similar to IFT_2. There is also a strong relationship (adjusted R^2 = 0.99) between the initial absorption coefficient (C(0)) and the photoreactive component (z_0) (Figure 4).

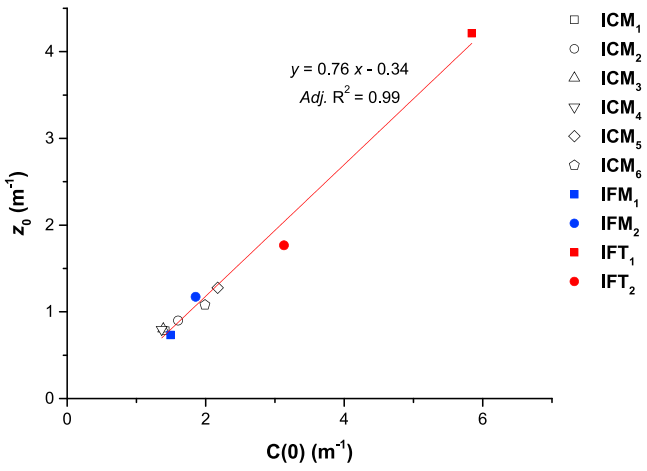

Figure 4. Relationship between the initial CDOM absorption coefficient at 254 nm (C (0)) and the photoreactive component (z_0) from the three-parameter exponential decay model.

Changes in DOM composition were also apparent during the 72 h irradiation experiments with clear shifts in the spectral slope parameters. For all experiments, $S_{275–295}$ decreased within the first 6 h of irradiation and then showed either little change or a slight increase at subsequent time points (Figure 5a). For most of the experiments, $S_{350–400}$ decreased over time or showed little change (Figure 5b). Over the full length of the experiment, 9 of the 10 experiments (except IFT_1) showed a statistically significant decrease ($p < 0.5$; two-tailed Student's

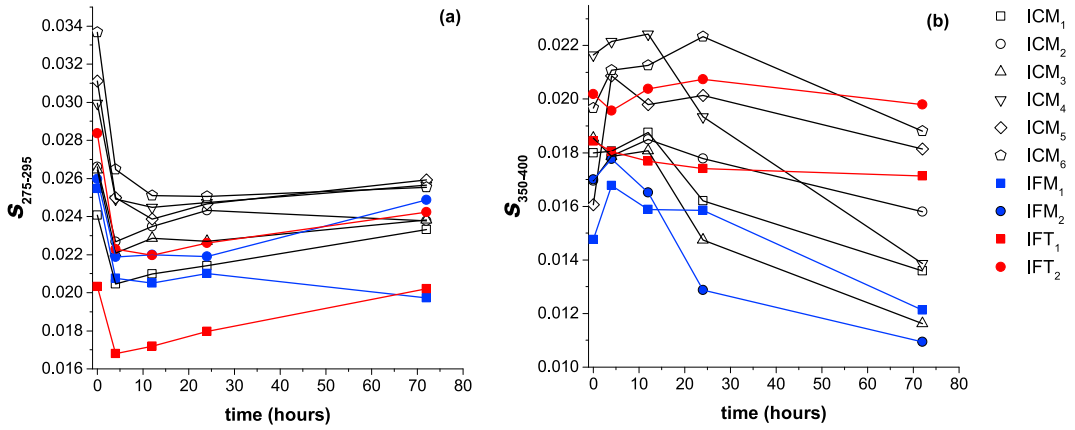

Figure 5. Changes in the spectral slopes (a) $S_{275–295}$ and (b) $S_{350–400}$ at each time interval for all experiments.

t test on triplicate samples from the beginning and end of each experiment) in $S_{275–295}$ (Table 4). For $S_{350–400}$, 9 of the 10 experiments (except ICM_5) also showed a statistically significant ($p < 0.5$) decrease (Table 4). Of the experiments that had a statistically significant change in S_R, all increased over the course of the experiment with the exception of ICM_6 (Table 4).

3.2. Photodegradation of FDOM and PARAFAC Results

An overall loss in total DOM fluorescence intensity was observed at the end of all experiments. Figure 6 shows EEMs from four representative experiments (ICM_1, IFM_1, IFT_1, and IFT_2) during the 72 h irradiation period. Under-ice marine samples had consistently lower initial FDOM intensities as compared to ice-free marine and terrestrially influenced samples. Furthermore, a greater proportion of the fluorescence signal was typically present at emission wavelengths less than 400 nm in the ICM and IFM samples, relative to the terrestrially influenced sites. The two terrestrially influenced samples clearly contained additional fluorescence signatures dominated by broad fluorescence peaks at emission wavelengths greater than 400 nm. Although all 10 samples showed an overall decay in FDOM intensity over the 72 h experiments, several samples showed an increase in total fluorescence intensity at intermediary time points (e.g., sample IFT_2 at t_4 in Figure 6), which then subsequently decayed.

Six independent fluorescent components were validated using PARAFAC analysis (Figure 7). Owing to the complex nature of DOM, it is unlikely that these components represent single fluorophores but instead represent a group of fluorophores that have similar properties and variability within the data set [*Baker and Spencer*, 2004; *Murphy et al.*, 2010; *Stubbins et al.*, 2014]. In particular, component 5 exhibited a shoulder that indicates that this component likely represents a mixture of fluorophores that the model was not able to separate because they covaried in the data set [*Stedmon and Markager*, 2005a]. The excitation and emission spectra of the components derived here are statistically compared to previously identified components in the OpenFluor database using the Tucker congruence coefficient in order to identify potential sources for each [*Murphy et al.*, 2014b]

Table 4. Initial, Final, and Percent Remaining After 72 h Irradiation Experiments for the Spectral Slope Parameters $S_{275–295}$, $S_{350–400}$, and S_R for All Experiments[a]

		ICM_1	ICM_2	ICM_3	ICM_4	ICM_5	ICM_6	IFM_1	IFM_2	IFT_1	IFT_2
$S_{275–295}$	Initial	0.0241	0.0266	0.0264	0.0299	0.0311	0.0337	0.0255	0.0260	0.0203	0.0284
	Final	0.0233	0.0238	0.0238	0.0257	0.0259	0.0255	0.0197	0.0249	0.0202	0.0242
	Difference	**−0.0008**	**−0.0028**	**−0.0026**	**−0.0043**	**−0.0052**	**−0.0081**	**−0.0057**	**−0.0011**	−0.0001	**−0.0041**
$S_{350–400}$	Initial	0.0180	0.0170	0.0185	0.0217	0.0161	0.0197	0.0148	0.0170	0.0184	0.0202
	Final	0.0136	0.0158	0.0116	0.0139	0.0181	0.0188	0.0121	0.0109	0.0171	0.0198
	Difference	**−0.0044**	**−0.0012**	**−0.0069**	**−0.0078**	0.0021	**−0.0009**	**−0.0026**	**−0.0060**	**−0.0013**	**−0.0004**
S_R	Initial	1.3371	1.5692	1.4257	1.3830	1.9370	1.7120	1.7253	1.5275	1.1029	1.4046
	Final	1.7154	1.5036	2.0480	1.8492	1.4288	1.3581	1.6264	2.2728	1.1793	1.2241
	Difference	**0.3783**	−0.0656	**0.6223**	**0.4662**	−0.5081	**−0.3539**	−0.0989	**0.7452**	**0.0764**	−0.1805

[a]Bold numbers indicate statistically significant ($p < 0.05$).

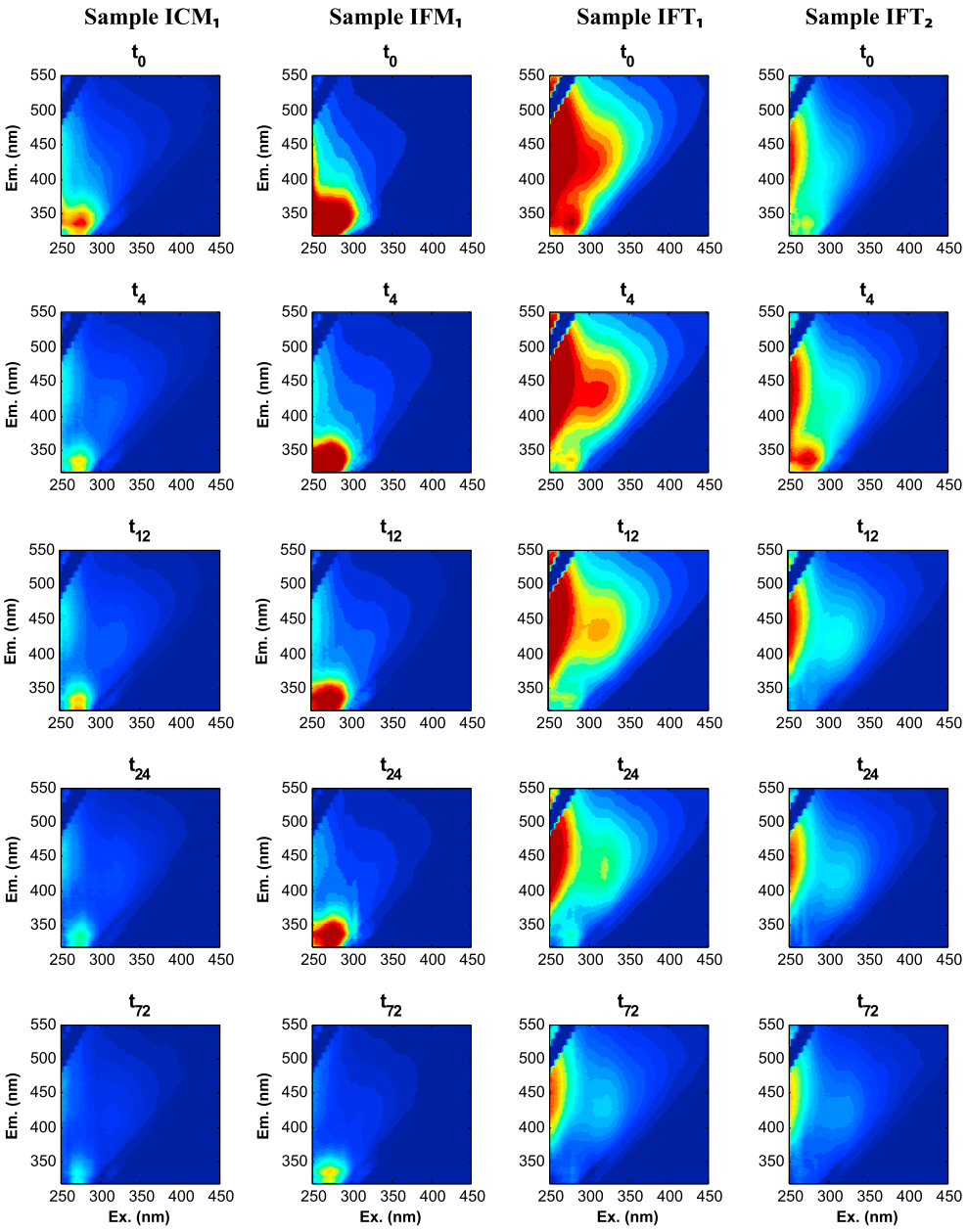

Figure 6. EEMs from a representative under-ice sample (ICM_1), ice-free marine sample (IFM_1), terrestrially influenced sample (IFT_1), and a sample that shows protein-like production (IFT_2).

(Table 5). Components 1, 3, 4, and 5 were statistically similar to other components in the database, and components 2 and 6 resembled components found in other studies (Table 5).

Components 1, 2, and 6 had spectra resembling humic-like DOM, with broad emission spectra around and above 400 nm and a broader excitation spectra compared to the other components (Figure 7). Components 1 and 2 exhibit characteristics of humic-like terrestrially derived material [*Stedmon and Markager*, 2005a, 2005b; *Stedmon et al.*, 2007a; *Kowalczuk et al.*, 2009; *Yamashita et al.*, 2010b; *Jørgensen et al.*, 2011; *Murphy et al.*, 2011; *Seredynska-Sobecka et al.*, 2011; *Shutova et al.*, 2014; *Tanaka et al.*, 2014]. Component 6 has also been identified as humic-like [*Stedmon and Markager*, 2005a; *Stedmon et al.*, 2007a; *Stedmon et al.*, 2007b; *Yamashita et al.*, 2010a; *Jørgensen et al.*, 2011], and *Stedmon and Markager* [2005a] categorized it as marine derived or anthropogenic in nature. Components 3, 4, and 5 exhibited spectra resembling "protein-like" DOM, with emission spectra maxima below 400 nm. Component 3 most closely resembles amino acids, free or bound in

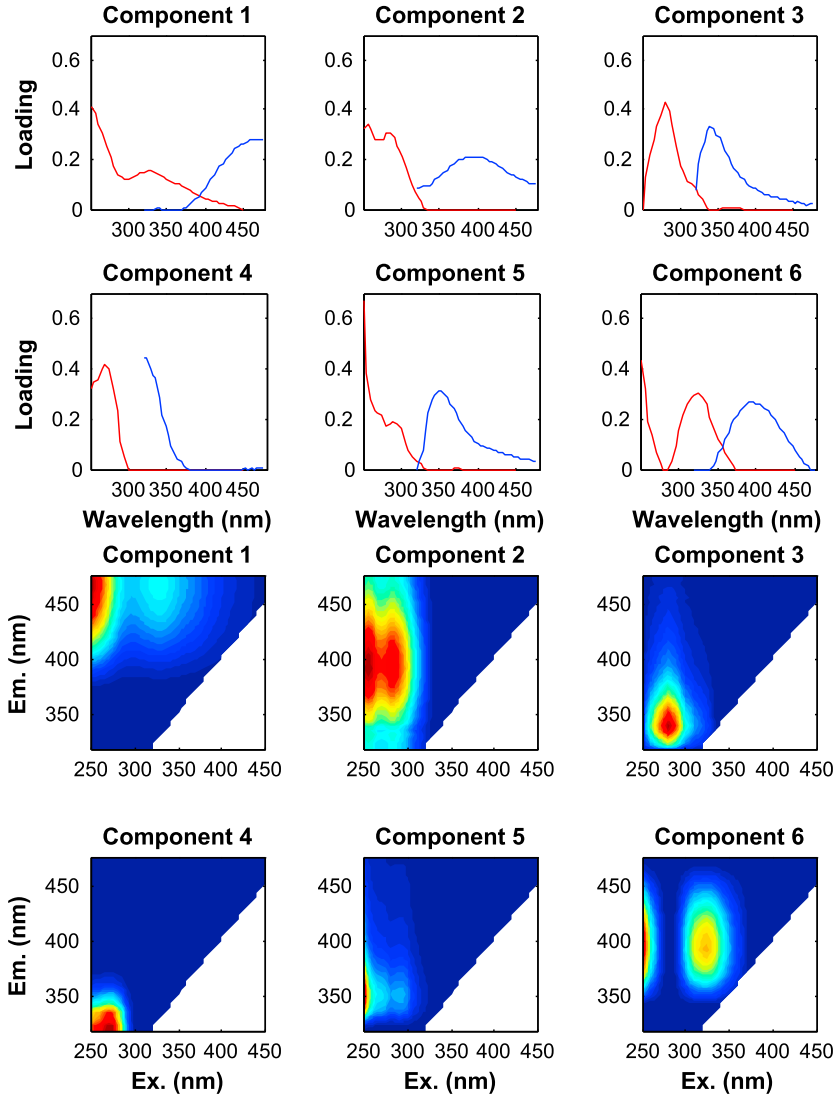

Figure 7. The six components for the PARAFAC model. The first and second rows show the excitation (red lines) and emission (blue lines) loadings for each component, and the third and fourth rows show the individual components.

proteins [*Murphy et al.*, 2008, 2014a], and component 4 resembles tyrosine [*Yamashita et al.*, 2011; *Graeber et al.*, 2012; *Yamashita et al.*, 2013], both of which are considered to be primarily microbially derived in marine waters [*Stedmon and Markager*, 2005b; *Coble*, 1996]. Component 5 is more difficult to classify; however, it is similar to component 6 in *Jørgensen et al.* [2011] that has been previously linked to surface water productivity.

Terrestrially influenced samples IFT_1 and IFT_2 had the highest overall fluorescence at the beginning of the experiments and were largely dominated by the humic-like component 1 (29–40% of initial fluorescence; Table 6). The IFM_1 sample was initially dominated by component 5 (48%) and also contained high levels of the protein-like components 3 (22%) and 4 (20%). The IFM_2 and under-ice samples generally exhibited low initial FDOM intensities with no clearly dominant fluorescent component. The exception was ICM_6, which exhibited greater contributions from component 4 (56%).

Distinct similarities and differences between sample types were observed with respect to how components changed over the 72 h irradiation experiments (Figure 8 and Table 6). In general, under-ice marine waters exhibited only small changes in each component with irradiation (typically less than 0.03 r.u.). For the ice-free marine samples, IFM_1 exhibited large changes in fluorescence in the three protein-like components, whereas IFM_2 showed little change in any component. For the terrestrially influenced samples, IFT_1 showed large

Table 5. Spectral Characteristics of the Six Components Identified by PARAFAC Compared to Previously Identified Components[a]

Components	Excitation Maxima (nm)	Emission Maxima (nm)	Other Studies	Description
1	<250 (330)	468	**C1 [*Jørgensen et al.*, 2011]** **C1 [*Kowalczuk et al.*, 2009]** **G1 [*Murphy et al.*, 2011]** **C3 [*Seredynska-Sobecka et al.*, 2011]** **C1 [*Shutova et al.*, 2014]** **C1 [*Stedmon and Markager*, 2005b]** **C1 [*Stedmon et al.*, 2007a]** **C1 [*Tanaka et al.*, 2014]** **C1 [*Yamashita et al.*, 2010b]**	humic-like, terrestrial
2	255 (280)	392	C3 [*Stedmon and Markager*, 2005a] C2 and C3 [*Stedmon and Markager*, 2005b]	humic-like, terrestrial
3	280	340	**C7 [*Murphy et al.*, 2008]** **C5 [*Murphy et al.*, 2014a]**	Amino acids, free or bound in proteins
4	270	320	**C7 [*Graeber et al.*, 2012]** **C4 [*Yamashita et al.*, 2011]** **C3 [*Yamashita et al.*, 2013]**	Protein- and tyrosine-like, positively related to bioavailability
5	<250	352	**C6 [*Jørgensen et al.*, 2011]**	protein-like, resembles free tryptophan
6	<250 (325)	392	C4 [*Jørgensen et al.*, 2011] C6 [*Stedmon and Markager*, 2005a] C2 [*Stedmon et al.*, 2007a] C3 [*Stedmon et al.*, 2007b] C2 [*Yamashita et al.*, 2010a]	humic-like, marine also common in wastewater and agricultural catchments

[a]Secondary maxima are shown in parentheses. Component matches (>0.95 tucker congruent coefficient) identified using the OpenFluor database (http://www.openfluor.org [*Murphy et al.*, 2014b]) are in bold. Matches not in bold were based on visual inspection.

losses in each component (55–99%) and IFT_2 exhibited large declines in components 2, 3, 4, and 5 (50–83%). Both IFT_1 and IFT_2 showed the greatest losses in "humic-like" components 4 and 5 (80–99%).

3.3. Photomineralization of DOC

DOC concentrations from the beginning and end of nine of the experiments are shown in Table 1 (sample loss prohibited measurement on the IFM_1 sample). Initial DOC concentrations in ICM and IFM samples were relatively low (53.6–71.9 μM), with higher concentrations in the two terrestrially influenced samples (105.4 and 80.5 μM). There was no apparent relationship between salinity and DOC. Of the nine experiments, only three (ICM_6, IFT_1, and IFT_2) showed a statistically significant ($p < 0.05$) change in DOC at the end of the 72 h irradiation period. Photomineralization losses were greatest in river-influenced samples, which showed an 8% (IFT_1) and 7% (IFT_2) decrease from initial DOC concentrations. The under-ice marine sample ICM_6 showed a 3% loss of DOC over this period. Overall losses in CDOM were far greater than for DOC

Table 6. Fluorescence Intensities (R.U.) of Individual Components Identified Using PARAFAC at the Beginning and End of the 72 h Irradiation

Components	ICM_1	ICM_2	ICM_3	ICM_4	ICM_5	ICM_6	IFM_1	IFM_2	IFT_1	IFT_2
1	0.022 (13)	0.026 (21)	0.022 (16)	0.019 (17)	0.027 (20)	0.021 (16)	0.022 (6)	0.036 (25)	0.136 (40)	0.049 (29)
	0.017 (27)	0.019 (23)	0.016 (26)	0.018 (20)	0.025 (22)	0.024 (43)	0.017 (17)	0.021 (17)	0.060 (56)	0.044 (48)
2	0.008 (5)	0.018 (15)	0.008 (6)	0.013 (11)	0.019 (14)	0.029 (22)	0.001 (0)	0.015 (10)	0.063 (18)	0.029 (17)
	0.004 (7)	0.005 (6)	0.004 (6)	0.005 (5)	0.008 (7)	0.008 (15)	0.000 (0)	0.003 (2)	0.015 (14)	0.014 (15)
3	0.037 (22)	0.020 (16)	0.031 (22)	0.016 (15)	0.020 (14)	0.000 (0)	0.085 (22)	0.026 (18)	0.030 (9)	0.011 (7)
	0.018 (28)	0.023 (28)	0.007 (12)	0.007 (8)	0.021 (19)	0.002 (4)	0.031 (31)	0.031 (25)	0.007 (7)	0.005 (6)
4	0.036 (21)	0.032 (26)	0.032 (23)	0.028 (25)	0.030 (21)	0.074 (56)	0.075 (20)	0.029 (20)	0.035 (10)	0.030 (18)
	0.017 (25)	0.017 (20)	0.014 (24)	0.023 (26)	0.006 (5)	0.007 (12)	0.034 (34)	0.026 (21)	0.004 (4)	0.006 (7)
5	0.054 (32)	0.014 (11)	0.037 (27)	0.028 (25)	0.031 (23)	0.000 (0)	0.180 (48)	0.021 (15)	0.037 (11)	0.032 (19)
	0.001 (1)	0.010 (12)	0.013 (21)	0.027 (31)	0.039 (35)	0.003 (5)	0.010 (10)	0.031 (26)	0.001 (0)	0.005 (6)
6	0.011 (7)	0.014 (11)	0.010 (7)	0.007 (6)	0.012 (8)	0.014 (7)	0.014 (4)	0.016 (11)	0.044 (13)	0.018 (11)
	0.008 (12)	0.009 (11)	0.007 (11)	0.008 (9)	0.013 (11)	0.008 (20)	0.008 (9)	0.011 (9)	0.020 (19)	0.018 (19)

[a]Percent of total fluorescence intensity is shown in parentheses.

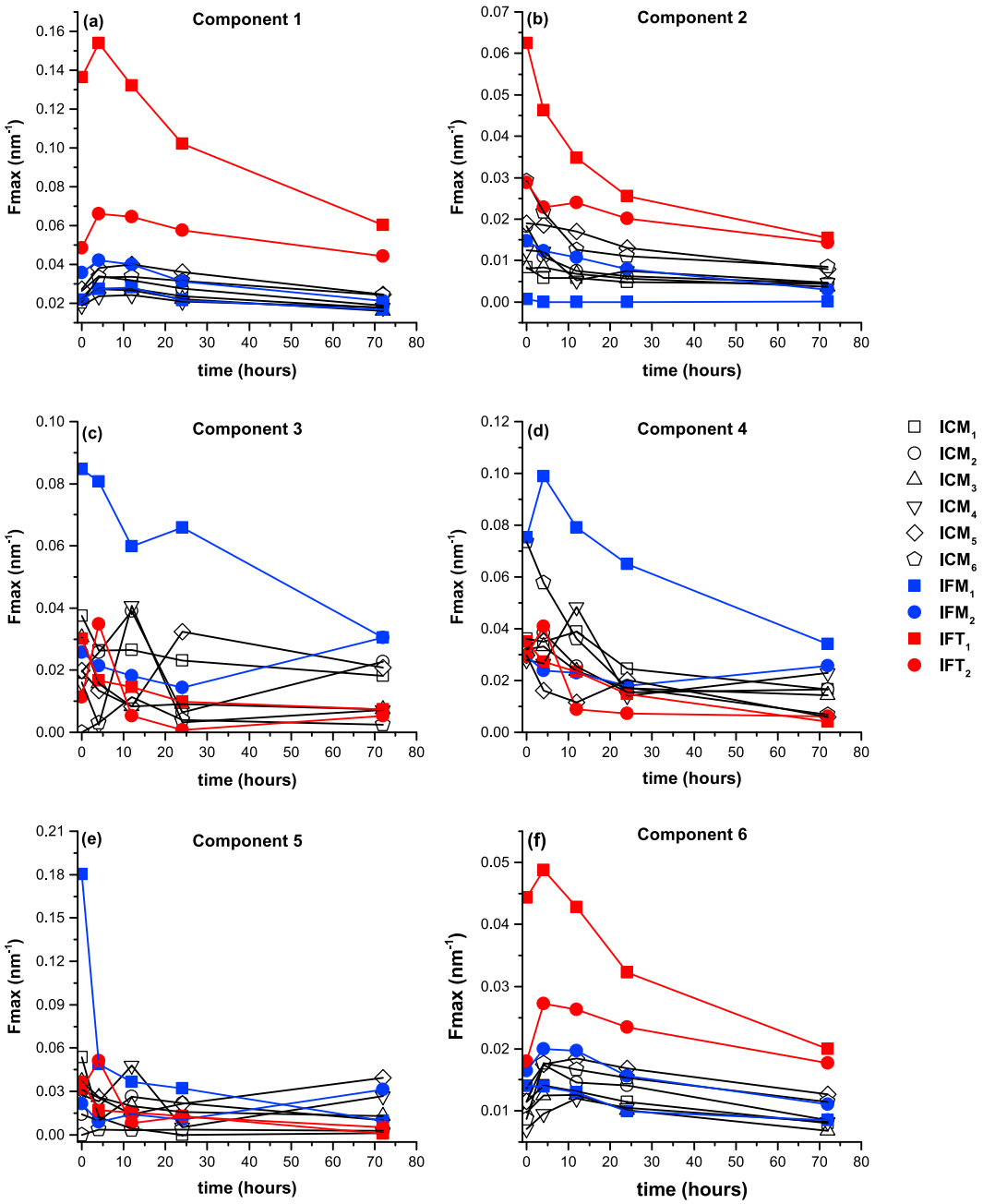

Figure 8. (a–f) Variability in fluorescence for the six PARAFAC components for all experiments over the 72 h irradiation experiments.

(Figure 9a). In particular, the percent loss in a_{254} ranged from ~48 to 62%, whereas the percent loss in DOC was only ~0 to 8% (Figure 9b).

4. Discussion

4.1. Impact of Photodegradation on CDOM From Sea Ice Melt

Initial CDOM absorption values were lower in ICM and IFM samples than in terrestrially influenced samples, in good agreement with many previous studies that report typically higher CDOM absorption in coastal, river-influenced regions than in open ocean regions [*Blough and Del Vecchio*, 2002; *Kitidis et al.*, 2006; *Osburn et al.*, 2009]. CDOM in the water column has been shown to be excluded from sea ice during formation

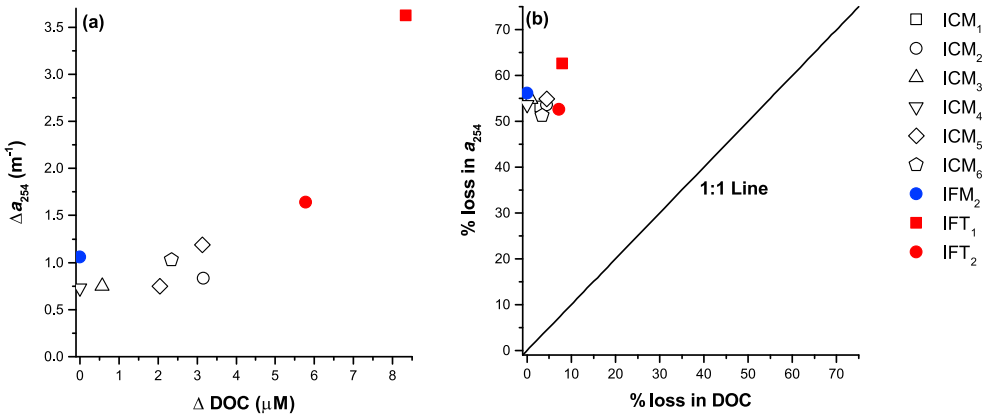

Figure 9. (a) Changes in CDOM absorbance at 254 nm as a function of the change in DOC after 72 h for all experiments. (b) Percent loss in CDOM absorbance at 254 nm after 72 h as a function of the percent loss in DOC for all experiments.

[*Amon*, 2003]. Therefore, in the absence of sea ice algae producing CDOM in situ [*Scully and Miller*, 2000], it would be expected that CDOM within sea ice melt would be low as well. The range in initial CDOM absorption values for ICM and IFM samples (1.36–2.17 m^{-1}) could be partially explained by the range in salinity (17.4–31.7), which suggests that DOM in these surface waters was of various sources and likely variable ages and residence times and therefore had undergone varying amounts of photochemical degradation prior to sampling. Despite differences in initial CDOM absorption values, CDOM was shown to be photoreactive irrespective of sampling location. Continuous losses of absorbance at 254 nm were observed (Figure 3a), suggesting that photochemical exposure caused the average aromatic content of the DOM pool to be progressively reduced during irradiation [*Osburn et al.*, 2001; *Stubbins et al.*, 2010; *Helms et al.*, 2014].

Photobleaching kinetics for a_{254} in these experiments are well described by three-parameter exponential decay models. Based on the photoreactive component (z_0) predicted to be lost after infinite photoexposure by these models, a_{254} could decrease by at least half for almost all of the samples if exposed to the Sun indefinitely, indicating that UV absorption by CDOM at these shorter wavelengths is diminished by photodegradation. However, these models indicated that, regardless of sample type or initial CDOM values, residual amounts (C_∞) of a_{254} (~0.57–0.91 m^{-1} for under-ice and ice-free marine samples and 1.36 and 1.63 m^{-1} for the two terrestrially influenced samples) would survive infinite photoexposure, suggesting that a persistent, yet small fraction of nonphotoreactive DOM (that absorbs shortwave UV) was present in all waters. Additionally, there is also a strong relationship (adjusted $R^2 = 0.99$) between the initial absorption coefficient ($C(0)$) and the photoreactive component (z_0) of all sample types (Figure 4) indicating that final a_{254} could potentially be predicted from initial measurements based on a regional model.

In our experiments, samples demonstrating significant changes in the spectral slope parameter generally exhibited decreases in both $S_{275–295}$ and $S_{350–400}$ and an increase in S_R during irradiation. For $S_{275–295}$ in particular, much of the change occurred within the first 6 h of the 72 h irradiation (Figure 5a) indicating rapid initial photoalteration in DOM composition. Similar to our experiments, *Helms et al.* [2008] showed increases in S_R and decreases in $S_{350–400}$; however, they showed that $S_{275–295}$ increased during their photodegradation experiments. In another study, *Spencer et al.* [2009] showed that (despite an initial increase in $S_{275–295}$) $S_{275–295}$ values decreased in Congo River DOM during irradiation after extensive light exposure. We suggest therefore that the decreases in $S_{275–295}$ in most of our samples may have been caused by extensive prior photodegradation in the environment, although these optical patterns may also derive from the freshly produced algal nature of CDOM in sea ice-impacted waters. For example, irradiation of CDOM from algal cultures can result in $S_{275–295}$ becoming shallower during photobleaching [*Bittar et al.*, 2015]. Changes in spectral slope parameters during irradiation have been related to changes in mean molecular weight [*Helms et al.*, 2008], where there have been particularly strong relationships between increases in S_R and decreases in average DOM molecular weight. Five of our experiments (ICM_1, ICM_3, ICM_4, IFM_2, and IFT_1) showed a significant increase in S_R during exposure. Based upon these results our samples may have undergone a significant decrease in mean DOM molecular weight during irradiation. However, the work by *Helms et al.* [2008] looked at

samples across a strong terrigenous-to-marine DOM gradient in the southeastern U.S., far from the current study site in terms of geography and biogeochemical system. Therefore, inferences about DOM quality based upon spectral slope and S_R in our current system must be interpreted with due caution until work shows that CDOM spectral qualities have similar empirical relationships to DOM quality in high latitude, sea ice-impacted surface waters.

4.2. Impact of Photodegradation on FDOM From Sea Ice Melt

A greater relative proportion of fluorescence at emission wavelengths less than 400 nm was typically present in each of the under-ice and ice-free marine samples, as compared to the terrestrially influenced sites. This is often referred to as protein-like fluorescence, has commonly been reported in marine samples [*Coble*, 1996; *Stedmon and Markager*, 2001], and appears to be associated with a family of low molecular weight molecules, including aliphatics and nitrogen-enriched aromatics [*Stubbins et al.*, 2014]. The two terrestrially influenced samples contained fluorescence signatures dominated by broad fluorescent peaks at emission wavelengths greater than 400 nm. This is typical of waters influenced by river runoff and commonly referred to as humic-like fluorescence [*Coble*, 1996; *Stedmon and Markager*, 2001; *Fellman et al.*, 2010]. These signatures have been associated with nitrogen-poor, relatively high mass molecular families [*Stubbins et al.*, 2014]. All 10 samples show an overall decay in FDOM intensity over the 72 h experiments, with the exception of protein-like production in several samples (occurring after 4 h in sample IFT_2; Figure 5), which subsequently decayed. Photo-induced production of tyrosine-like fluorescence (which contributes to the protein-like fluorescence signal) has been previously observed in lacustrine [*Stedmon et al.*, 2007a] and marine waters [*Mann*, 2010].

PARAFAC decomposition identified six components, and overall, these fluorescent components were shown to decay, or remain constant, over the course of the experiments. Under-ice and ice-free marine waters were dominated by the protein-like components, whereas terrestrially influenced samples contained higher proportions of the humic-like fluorophores (Figure 8 and Table 5). All components were shown to be photoreactive in at least one of our experiments, further demonstrating that DOM irrespective of source was susceptible to photobleaching. Under-ice and ice-free marine waters showed the greatest decreases in FDOM of protein-like components (which are associated with recently algal-produced labile DOM), whereas the greatest decreases in the terrestrially influenced samples occurred in humic-like components.

Studies have indicated that photodegradation of DOM can result in increasing [*Moran and Zepp*, 1997] or decreasing biological lability [*Tranvik and Kokalj*, 1998] depending on DOM source. In general, both field and laboratory studies suggest that photodegradation causes humic-rich DOM to become more bioavailable, whereas recently produced algal-derived DOM in surface waters becomes less biolabile [*Benner and Biddanda*, 1998; *Obernosterer et al.*, 1999, 2001; *Tranvik et al.*, 1999; *Tranvik and Bertilsson*, 2001; *Bittar et al.*, 2015]. In particular, protein-like fluorescence of algal origin has been shown to be both biolabile and photolabile, indicating that these two processes compete to mineralize fresh, algal DOC [*Stedmon and Markager*, 2005b; *Bittar et al.*, 2015]. Based on our FDOM analyses, the majority of CDOM in under-ice and ice-free marine waters appears to be algal-derived; therefore, we may expect photoirradiation of these waters to reduce the availability of biolabile DOC through direct photomineralization and through photoalteration to less biolabile material as found for DOM produced by algal cultures [*Bittar et al.*, 2015]. Thus, photochemistry of algal-derived DOM in sea ice systems may short circuit the microbial loop, whereas photodegradation of terrigenous DOM is likely to increase DOM biolability and enhance bacterioplankton productivity.

4.3. Photobleaching Versus Photomineralization

Three of our samples displayed significant changes in DOC concentration with irradiation. The three samples (ICM_6, IFT_1, and IFT_2) were all from the easternmost transect that was closest to the mouth of the Colville River and were likely influenced by the relatively high-DOC, high-CDOM riverine water runoff. Investigating the various components identified in the PARAFAC analysis, changes in component 2 (identified as humic-like and terrestrially derived; Table 5) had the strongest significant correlation with changes in DOC ($R = 0.78$, $p < 0.02$), indicating that there may be a link between this component and DOC. These results suggest that as melt ponds form and sea ice retreats, terrestrial DOM below the ice would be susceptible to photomineralization to dissolved inorganic carbon.

Our experiments suggest that it is not possible to calculate DOC from CDOM using a constant, linear relationship in the Chukchi and Beaufort Seas. Several methods for using CDOM measurements as a proxy for DOC

have previously been proposed [*Ferrari et al.*, 1996; *Del Vecchio and Blough*, 2004; *Gueguen et al.*, 2005] because CDOM can be measured at a much higher spatial resolution using remote sensing and at a high temporal resolution using in situ measurements, and as such, it has the potential to more easily provide broader spatial and temporal coverage. A promising new approach was suggested by *Fichot and Benner* [2011], which derives DOC concentrations from CDOM absorption coefficients at 275 and 295 nm, and their approach worked well for the coastal waters of the Beaufort Sea (eastward of our study area). However, based on the results of our photodegradation experiments, the method is likely not applicable for the nearby under-ice and ice-free marine waters (that are less influenced by river runoff), as while there were measurable changes in the absorption coefficients at shorter wavelengths with irradiation, there were no measurable changes in DOC.

Photodegradation resulted in measurable changes in the optical properties of DOM in all sample waters, yet none of the ice-free and under-ice marine samples from the westernmost and central transects showed a significant change in DOC with irradiation. Several studies have shown that photochemical loss of DOC is less efficient than CDOM photobleaching [*Moran et al.*, 2000; *Vahatalo and Wetzel*, 2004; *Spencer et al.*, 2009]. Furthermore, *Osburn et al.* [2009] conducted photoreactivity experiments on water samples from the Mackenzie River, estuary, shelf, and gulf regions of the western Canadian Arctic and found less than 1% loss in DOC after 3 days in ambient Arctic sunlight. Similar results were found for sea ice brine from Antarctic sea ice [*Norman et al.*, 2011]. The absence of measurable changes in DOC in waters in the westernmost and central transects in this study indicates that either there is a decoupling between CDOM photobleaching and DOC photomineralization or that any changes in DOC were below the detection limit of our instrument.

Photochemistry can result in the production of CO_2 through two different pathways: (a) the abiotic photomineralization of DOC into CO_2 and CO and (b) a photochemical-biotic pathway through which photodegradation alters the bioavailability of DOM potentially making it more labile, allowing it to be consumed by bacteria and converted into biomass and CO_2 (see sources in *Mopper et al.* [2015]). Not only was there very little photomineralization evident in the western and central transects in our study but the changes in spectral slopes and fluorescence components observed in these experiments suggest that there may have been an overall reduction in the biolability of DOM in under-ice and marine surface waters. Therefore, it appears that photodegradation of marine waters and sea ice melt does not result in significant outgassing of CO_2 to the atmosphere via either the purely photochemical pathway or the combined photochemical-biological pathway. Results presented here suggest that photodegradation of under-ice waters is far more important for photobleaching (and changes in light penetration in the euphotic zone) than it is for carbon cycling.

5. Implications and Conclusions

As the Arctic continues to warm and sea ice extent declines, the photoreactivity of DOM may have important implications for primary productivity and the heat balance of the Arctic Ocean. Thirty years ago much of the Arctic Ocean was covered with thick multiyear ice throughout the summer [*Serreze et al.*, 2007; *Kwok and Rothrock*, 2009], which limited the amount of UV and visible light reaching under-ice waters. With decreasing sea ice extent and increases in thin first-year ice and surface melt ponds, the surface layer of the Arctic Ocean is being exposed to more solar radiation during the summer melt season. Several studies suggest that primary productivity will increase in Arctic waters owing to this decrease in sea ice extent [*Arrigo et al.*, 2008; *Arrigo and van Dijken*, 2011] and increase in melt pond coverage [*Arrigo et al.*, 2012] and the corresponding increase in PAR reaching ocean surface waters. However, continued ponding, thinning, and ultimate loss of summer sea ice cover would also lead to a decrease in UV absorption by surface CDOM with photodegradation. Combined with the unprecedented loss in Arctic ozone in recent years [*Solomon et al.*, 2007; *Manney et al.*, 2011], this may result in exposure of marine organisms to more harmful UV radiation and may in turn negatively impact primary productivity. An additional complication is that the decrease in sea ice extent and increase in open water during the summer months have been shown to coincide with an increase in cloud coverage [*Wang and Key*, 2005; *Eastman and Warren*, 2010; *Palm et al.*, 2010], which limits the amount of shortwave radiation reaching the ocean surface. Models show that these trends will likely continue in the future [*Vavrus et al.*, 2010], potentially counteracting the increase in UV exposure owing to changes in sea ice but also limiting the amount of available PAR [*Belanger et al.*, 2013]. This presents challenges for predicting

future trends in the amount of UV and visible radiation reaching surface waters and quantifying the overall impact that CDOM photodegradation will have on primary production.

Warming temperatures in the Arctic are leading to permafrost thaw [*Romanovsky et al.*, 2010] and increases in riverine discharge [*Peterson et al.*, 2002], which in turn will likely lead to increases in terrestrial DOM output to surface waters of the Arctic Ocean [*Frey and McClelland*, 2009]. Our results suggest that increasing terrestrial DOM supply will result in a measureable increase in DOM photodegradation and loss of DOC, since significant changes in DOC were observed in samples exhibiting greater contributions from humic-like terrestrially sourced FDOM components. Increases in daily minimum flow rates, particularly in winter, have been shown for Arctic rivers [*Smith et al.*, 2007], which could potentially increase the amount of terrestrial DOM transported to surface waters of the Arctic Ocean [*Holmes et al.*, 2008; *Stedmon et al.*, 2011]. Since this would occur when there is little light north of the Arctic Circle and the Arctic Ocean is largely covered in sea ice, this DOM would initially be protected from photodegradation and could be transported well into shelf seas and possibly the Arctic Ocean basin interior. Furthermore, the spring freshet period has been shown to export a major fraction of the annual DOM load of Arctic rivers and DOM exported during this period is relatively more aromatic in character and more photolabile in comparison to other times of year [*Spencer et al.*, 2008; *Holmes et al.*, 2012; *Mann et al.*, 2012]. This major pulse of photoreactive DOM enters the Arctic Ocean at the onset of spring, and thus, with the decrease in sea ice extent and increase in melt ponding during the following spring and summer, our results suggest that this DOM would be poised for significant photodegradation during the subsequent melt season. This combined with increased DOM from under-ice blooms, and subsequent photodegradation could alter CO_2 saturation in surface waters.

By absorbing sunlight and subsequently reemitting it as heat, CDOM also contributes to the heating of surface waters [*Kirk*, 1988]. With increasing sea ice melt, more light may be transmitted through sea ice and absorbed and emitted as heat by the existing CDOM below. This increase in heat absorption by the under-ice water column could increase local sea surface temperatures and potentially lead to further sea ice melt from below, thus initiating a positive feedback to sea ice melt [*Hill*, 2008]. A future increase in CDOM supply, particularly from riverine sources, would considerably increase CDOM absorption, and it is likely that photodegradation will substantially decrease the light absorption of this additional riverine CDOM. At present, the combined effect of increases in CDOM additions from in situ production and riverine sources as well as increasing CDOM photobleaching as ice cover recedes upon ocean surface heating remain unclear.

In conclusion, our observed reductions in CDOM absorbance at shorter wavelengths suggest that the beneficial UV protection currently received by marine organisms may significantly reduce with sea ice melt ponding and overall declines of sea ice cover. However, some of these CDOM losses may be balanced by increasing CDOM inputs from increased primary production and terrestrial carbon export. We additionally show that under current conditions, photodegradation of CDOM in under-ice waters is not a significant source of CO_2, and it is unclear whether the potential for surface ocean heating is compromised with irradiation. However, as Arctic temperatures warm and summer sea ice continues to disappear, continued examination of the resulting enhanced photodegradation processes and their impacts on the interplay between primary production, carbon biogeochemistry, and surface ocean heating will be vital.

Acknowledgments

All data in this study are currently available either in tables within this manuscript or upon request from the corresponding author (kfrey@clarku.edu) and will additionally be available at the ACADIS Arctic Data Repository (http://www.aoncadis.org). This research was part of the NASA Impacts of Climate Change on the Ecosystems and Chemistry of the Arctic Pacific Environment (ICESCAPE) project with support from the NASA Cryospheric Sciences Program (grants NNX10AH71G and NNX14AH61G to K. Frey) and the NASA Ocean Biology and Biogeochemistry Program. The field component of this research would not have been possible without the tremendous support from the commanding officer, marine science technicians, crew, and officers of USCGC *Healy* on the HLY1101 mission to the Chukchi and Beaufort Seas in June–July 2011. We thank Leanne Powers for the assistance in generating modeled solar irradiance data. Additional funding was provided by NSF DEB-1146161 to A. Stubbins and NSF ANT-1203885/PLR-1500169 to R. Spencer.

References

Amon, R. M. W. (2003), The role of dissolved organic matter for the organic carbon cycle in the Arctic Ocean, in *The Organic Carbon Cycle in the Arctic Ocean*, edited by R. Stein and R. MacDonald, pp. 83–99, Springer, Berlin.

Arrigo, K. R., and G. L. van Dijken (2011), Secular trends in Arctic Ocean net primary production, *J. Geophys. Res.*, *116*, C09011, doi:10.1029/2011JC007151.

Arrigo, K. R., G. van Dijken, and S. Pabi (2008), Impact of a shrinking Arctic ice cover on marine primary production, *Geophys. Res. Lett.*, *35*, L19603, doi:10.1029/2008GL035028.

Arrigo, K. R., et al. (2012), Massive phytoplankton blooms under Arctic sea ice, *Science*, *336*, 1407–1408.

Baker, A., and R. G. M. Spencer (2004), Characterization of dissolved organic matter from source to sea using fluorescence and absorbance spectroscopy, *Sci. Total Environ.*, *333*, 217–232.

Belanger, S., H. Xie, N. Krotkov, and P. Larouche (2006), Photomineralization of terrigenous dissolved organic matter in Arctic coastal waters from 1979 to2003: Interannual variability and implications of climate change, *Global Biogeochem. Cycles*, *20*, GB4005, doi:10.1029/2006GB002708.

Belanger, S., M. Babin, and J.-E. Tremblay (2013), Increasing cloudiness in Arctic damps the increase in phytoplankton primary production due to sea ice receding, *Biogeosciences*, *10*, 4087–4101, doi:10.5194/bg-10-4087-2013.

Benner, R., and B. Biddanda (1998), Photochemical transformations of surface and deep marine dissolved organic matter: Effects on bacterial growth, *Limnol. Oceanogr.*, *43*(6), 1373–1378.

Bittar, T. B., A. A. H. Vieira, A. Stubbins, and K. Mopper (2015), Competition between photochemical and biological degradation of dissolved organic matter from the cyanobacteria Microcystis aeruginosa, *Limnol. Oceanogr.*, *60*(4), 1172–1194.
Blough, N. V., and R. Del Vecchio (2002), Chromophoic DOM in the coastal environment, in *Biogeochemistry of Marine Dissolved Organic Matter*, edited by D. A. Hansell and C. A. Carlson, pp. 509–546, Elsevier, San Diego, Calif.
Brown, M. (1977), Transmission spectroscopy examinations of natural waters, *Estuarine Coastal Mar. Sci.*, *5*, 309–317, doi:10.1016/0302-3524(77)90058-5.
Carlson, C. A. (2002), Production and removal processes, in *Biogeochemistry of Marine Dissolved Organic Matter*, edited by D. A. Hansell and C. A. Carlson, pp. 91–151, Elsevier, San Diego, Calif.
Coble, P. G. (1996), Characterization of marine and terrestrial DOM in seawater using excitation-emission matrix spectroscopy, *Mar. Chem.*, *51*, 325–346.
Coble, P. G. (2007), Marine optical biogeochemistry: The chemistry of ocean color, *Chem. Rev.*, *107*, 402–418.
Comiso, J. C. (2012), Large decadal decline of the Arctic multiyear ice cover, *J. Clim.*, *25*(4), 1176–1193, doi:10.1175/JCLI-D-11-00113.1.
Comiso, J. C., C. L. Parkinson, R. Gersten, and L. Stock (2008), Accelerated decline in the Arctic sea ice cover, *Geophys. Res. Lett.*, *35*, L01703, doi:10.1029/2007GL031972.
Del Vecchio, R., and N. V. Blough (2004), Spatial and seasonal distribution of chromophoric dissolved organic matter and dissolved organic carbon in the Middle Atlantic Bight, *Mar. Chem.*, *89*(1–4), 169–187, doi:10.1016/j.marchem.2004.02.027.
Dittmar, T., and G. Kattner (2003), The biogeochemistry of the river and shelf ecosystem of the Arctic Ocean: A review, *Mar. Chem.*, *83*, 103–120, doi:10.1016/S0304-4203(03)00105-1.
Eastman, R., and S. G. Warren (2010), Arctic cloud changes from surface and satellite observations, *J. Clim.*, *23*, 4233–4242, doi:10.1175/2010JCLI3544.1.
Fellman, J. R., E. Hood, and R. G. M. Spencer (2010), Fluorescence spectroscopy opens new windows into dissolved organic matter dynamics in freshwater ecosystems: A review, *Limnol. Oceanogr.*, *55*, 2452–2462.
Ferrari, G. M., M. D. Dowell, S. Grossi, and C. Targa (1996), Relationship between the optical properties of chromophoric dissolved organic matter and total concentration of dissolved organic carbon in the southern Baltic Sea region, *Mar. Chem.*, *55*(3–4), 299–316.
Fetterer, F., and N. Untersteiner (1998), Observations of melt ponds on Arctic sea ice, *J. Geophys. Res.*, *103*(C11), 24, 821–24,835, doi:10.1029/98JC02034.
Fichot, C. G., and R. Benner (2011), A novel method to estimate DOC concentrations from CDOM absorption coefficients in coastal waters, *Geophys. Res. Lett.*, *38*, L03610, doi:10.1029/2010GL046152.
Frey, K. E., and J. W. McClelland (2009), Impacts of permafrost degradation on Arctic river biogeochemistry, *Hydrol. Processes*, *23*, 169–182, doi:10.1002/hyp.7196.
Frey, K. E., D. K. Perovich, and B. Light (2011), The spatial distribution of solar radiation under a melting Arctic sea ice cover, *Geophys. Res. Lett.*, *38*, L22501, doi:10.1029/2011GL049421.
Graeber, D., J. Gelbrecht, M. Pusch, C. Anlanger, and D. von Schiller (2012), Agriculture has changed the amount and composition of dissolved organic matter in central European headwater streams, *Sci. Total Environ.*, *438*, 435–446.
Granskog, M. A., R. W. Macdonald, C. J. Mundy, and D. G. Barber (2007), Distribution, characteristics and potential impacts of chromophoric dissolved organic matter (CDOM) in Hudson Strait and Hudson Bay, Canada, *Cont. Shelf Res.*, *27*, 2032–2050, doi:10.1016/j.csr.2007.05.001.
Green, S. A., and N. V. Blough (1994), Optical absorption and fluorescence properties of chromophoric dissolved organic matter in natural waters, *Limnol. Oceanogr.*, *39*, 1903–1916.
Gueguen, C., L. Guo, and N. Tanaka (2005), Ditributions and characteristics of colored dissolved organic matter in the western Arctic Ocean, *Cont. Shelf Res.*, *25*, 1195–1207, doi:10.1016/j.csr.2005.01.005.
Gueguen, C., L. Guo, M. Yamamoto-Kawai, and N. Tanaka (2007), Colored dissolved organic matter dynamics across the shelf-basin interface in the western Arctic Ocean, *J. Geophys. Res.*, *112*, C05038, doi:10.1029/2006JC003584.
Helms, J. R., A. Stubbins, J. D. Ritchie, E. C. Minor, D. J. Kieber, and K. Mopper (2008), Absorption spectral slopes, and slope ratios as indicators of molecular weight, source, and photobleaching of chromophoric dissolved organic matter, *Limnol. Oceanogr.*, *53*, 955–969.
Helms, J. R., J. Mao, A. Stubbins, K. Schmidt-Rohr, R. G. M. Spencer, P. J. Hernes, and K. Mopper (2014), Loss of optical and molecular indicators of terrigenous dissolved organic matter during long-term photobleaching, *Aquat. Sci.*, *76*(3), 353–373.
Hill, V. J. (2008), Impacts of chromophoric dissolved organic material on surface ocean heating in the Chukchi Sea, *J. Geophys. Res.*, *113*, C07024, doi:10.1029/2007JC004119.
Holmes, R. M., J. W. McClelland, P. A. Raymond, B. B. Frazer, B. J. Peterson, and M. Stieglitz (2008), Lability of DOC transported by Alaskan Rivers to the Arctic Ocean, *Geophys. Res. Lett.*, *35*, L03402, doi:10.1029/2007GL032837.
Holmes, R. M., et al. (2012), Seasonal and annual fluxes of nutrients and organic matter from large rivers to the Arctic Ocean and surrounding seas, *Estuaries Coasts*, *35*, 369–382, doi:10.1007/s12237-011-9386-6.
Jørgensen, L., C. A. Stedmon, T. Kragh, S. Markager, M. Middelboe, and M. Søndergaard (2011), Global trends in the fluorescence characteristics and distribution of marine dissolved organic matter, *Mar. Chem.*, *126*, 139–148, doi:10.1016/j.marchem.2011.05.002.
Kirk, J. T. O. (1988), Solar heating of water bodies as influenced by their inherent optical properties, *J. Geophys. Res.*, *93*(D9), 10,897–10,908, doi:10.1029/JD093iD09p10897.
Kirk, J. T. O. (1994), *Light and Photosynthesis in Aquatic Ecosystems*, Cambridge Univ. Press, Cambridge, U. K.
Kitidis, V., A. P. Stubbins, G. Uher, R. C. U. Goddard, C. S. Law, and E. M. S. Woodward (2006), Variability of chromophoric organic matter in surface waters of the Atlantic Ocean, *Deep Sea Res., Part II*, *53*(14), 1666–1684.
Kowalczuk, P., M. J. Durako, H. Young, A. E. Kahn, W. J. Cooper, and M. Gonsior (2009), Characterization of dissolved organic matter fluorescence in the South Atlantic Bight with use of PARAFAC model: Interannual variability, *Mar. Chem.*, *113*, 182–196.
Kwok, R., and D. A. Rothrock (2009), Decline in Arctic sea ice thickness from submarine and ICESat records: 1958–2008, *Geophys. Res. Lett.*, *36*, L15501, doi:10.1029/2009GL039035.
Lawaektz, A. J., and C. A. Stedmon (2009), Fluorescence intensity calibration using the Raman scatter peak of water, *Appl. Spectrosc.*, *63*(8), 936–940.
Light, B., T. C. Grenfell, and D. K. Perovich (2008), Transmission and absorption of solar radiation by Arctic sea ice during the melt season, *J. Geophys. Res.*, *113*, C03023, doi:10.1029/206JC003977.
Mann, P. J. (2010), Ammonium photoproduction and CDOM biogeochemistry in marine systems, PhD thesis. Newcastle Univ., U. K.
Mann, P. J., A. Davidova, N. Zimov, R. G. M. Spencer, S. Davydov, E. Bulygina, S. Zimov, and R. M. Holmes (2012), Controls on the composition and lability of dissolved organic matter in Siberia's Kolyma River basin, *J. Geophys. Res.*, *117*, G01028, doi:10.1029/2011JG001798.
Manney, G. L., et al. (2011), Unprecedented Arctic ozone loss in 2011, *Nature*, *478*, 469–475, doi:10.1038/nature10556.
Markus, T., J. C. Stroeve, and J. Miller (2009), Recent changes in Arctic sea ice melt onset, freezeup, and melt season length, *J. Geophys. Res.*, *114*, C12024, doi:10.1029/2009JC005436.

Maslanik, J. A., C. Fowler, J. Stroeve, S. Drobot, J. Zwally, D. Yi, and W. Emery (2007), A younger, thinner Arctic ice cover: Increased potential for rapid, extensive sea-ice loss, *Geophys. Res. Lett.*, *34*, L24501, doi:10.1029/2007GL032043.

Maslanik, J., J. Stroeve, C. Fowler, and W. Emery (2011), Distribution and trends in Arctic sea ice age through spring 2011, *Geophys. Res. Lett.*, *38*, L13502, doi:10.1029/2011GL047735.

Matsuoka, A., Y. Huot, K. Shimada, S. Saitoh, and M. Babin (2007), Bio-optical characteristics of the western Arctic Ocean: Implications for ocean color algorithms, *Can. J. Remote Sens.*, *33*(6), 503–518.

Matsuoka, A., V. Hill, Y. Huot, M. Babin, and A. Bricaud (2011), Seasonal variability in the light absorption properties of western Arctic waters: Parameterization of the individual components of absorption for ocean color applications, *J. Geophys. Res.*, *116*, C02007, doi:10.1029/2009JC005594.

Mopper, K., D. Kieber, and A. Stubbins (2015), Marine photochemistry: Processes and impacts, in *Biogeochemistry of Marine Dissolved Organic Matter*, edited by D. A. Hansell and C. A. Carlson, 2nd ed., Elsevier, San Diego, Calif.

Moran, M. A., and R. G. Zepp (1997), Role of photoreactions in the formation of biologically labile compounds from dissolved organic matter, *Limnol. Oceanogr.*, *42*, 1307–1316.

Moran, M. A., W. M. Sheldon, and R. G. Zepp (2000), Carbon loss and optical property changes during long-term photochemical and biological degradation of estuarine dissolved organic matter, *Limnol. Oceanogr.*, *45*(6), 1254–1264.

Murphy, K. R., C. A. Stedmon, T. D. Waite, and G. M. Ruiz (2008), Distinguishing between terrestrial and autochthonous organic matter sources in marine environments using fluorescence spectroscopy, *Mar. Chem.*, *108*, 40–58.

Murphy, K. R., K. D. Butler, R. G. M. Spencer, C. A. Stedmon, J. R. Boehme, and G. R. Aiken (2010), Measurement of dissolved organic matter fluorescence in aquatic environments: An interlaboratory comparison, *Environ. Sci. Technol.*, *44*, 9405–9412.

Murphy, K. R., A. Hambly, S. Singh, R. K. Henderson, A. Baker, R. Stuetz, and S. J. Khan (2011), Organic matter fluorescence in municipal water recycling schemes: Toward a unified PARAFAC model, *Environ. Sci. Technol.*, *45*, 2909–2916.

Murphy, K. R., R. Bro, and C. A. Stedmon (2014a), Chemometric analysis of organic matter fluorescence, in *Aquatic Organic Matter Fluorescence*, edited by P. Coble et al., Cambridge Univ. Press, New York.

Murphy, K. R., C. A. Stedmon, P. Wenig, and R. Bro (2014b), OpenFluor—A spectral database of auto-fluorescence by organic compounds in the environment, *Anal. Methods*, *6*, 658–661, doi:10.1039/C3AY41935E.

Nelson, N. B., and D. A. Siegel (2002), Chromophoric DOM in the open ocean, in *Biogeochemistry of Marine Dissolved Organic Matter*, edited by D. A. Hansell and C. A. Carlson, pp. 547–578, Elsevier, San Diego, Calif.

Nicolaus, M., C. Katlein, J. Maslanik, and S. Hendricks (2012), Changes in Arctic sea ice result in increasing light transmittance and absorption, *Geophys. Res. Lett.*, *39*, L24501, doi:10.1029/2012GL053738.

Norman, L., D. N. Thomas, C. A. Stedmon, M. A. Granskog, S. Papadimitriou, R. Krapp, K. M. Meiners, D. Lannuzel, P. van der Merwe, and G. S. Dieckmann (2011), The characteristics of chromophoric dissolved organic matter (CDOM) in Antarctic sea ice, *Deep Sea Res., Part II*, *58*, 1075–1091, doi:10.1016/j.dsr2.2010.10.030.

Obernosterer, I., B. Reitner, and G. Herndl (1999), Contrasting effects of solar radiation on dissolved organic matter and its bioavailability to marine bacterioplankton, *Limnol. Oceanogr.*, *44*(7), 1645–1654.

Obernosterer, I., R. Sempere, and G. J. Herndl (2001), Ultraviolet radiation induces reversal of the bioavailability of DOM to marine bacterioplankton, *Aquat. Microb. Ecol.*, *24*(1), 61–68.

Opsahl, S., R. Benner, and R. M. Amon (1999), Major flux of terrigenous dissolved organic matter through the Arctic Ocean, *Limnol. Oceanogr.*, *44*(8), 2017–2023, doi:10.4319/lo.1999.44.8.2017.

Osburn, C. L., D. P. Morris, K. A. Thorn, and R. E. Moeller (2001), Chemical and optical changes in freshwater dissolved organic matter exposed to solar radiation, *Biogeochemistry*, *54*(3), 251–278.

Osburn, C. L., L. Retamal, and W. F. Vincent (2009), Photoreactivity of chromophoric dissolved organic matter transported by the Mackenzie River to the Beaufort Sea, *Mar. Chem.*, *115*, 10–20, doi:10.1016/j.marchem.2009.05.003.

Palm, S. P., S. T. Strey, J. Spinhirne, and T. Markus (2010), Influence of Arctic sea ice extent on polar cloud fraction and vertical structure and implications for regional climate, *J. Geophys. Res.*, *115*, D21209, doi:10.1029/2010JD013900.

Pegau, W. S. (2002), Inherent optical properties of the central Arctic surface waters, *J. Geophys. Res.*, *107*(C10), 8035, doi:10.1029/2000JC000382.

Perovich, D. K., B. Light, H. Eicken, K. F. Jones, K. Runciman, and S. V. Nghiem (2007), Increasing solar heating of the Arctic Ocean and adjacent seas, 1979–2005: Attribution and role in the ice-albedo feedback, *Geophys. Res. Lett.*, *34*, L19505, doi:10.1029/2007GL031480.

Perovich, D., W. Meier, M. Tschudi, S. Gerland, and J. Richter-Menge (2012), Sea ice [In Arctic Report Card 2012]. [Available at http://www.arctic.noaa.gov/reportcard.]

Peterson, B. J., R. M. Holmes, J. W. McClelland, C. J. Vorosmarty, I. A. Shiklomonov, R. B. Lammers, and S. Rahmstorf (2002), Increasing river discharge to the Arctic Ocean, *Science*, *298*, 2171–2173.

Powers, L. C., and W. L. Miller (2015), Photochemical production of CO and CO_2 in the Northern Gulf of Mexico: Estimates and challenges for quantifying the impact of photochemistry on carbon cycles, *Mar. Chem.*, *171*, 21–35.

Raymond, P. A., and R. G. M. Spencer (2015), Riverine DOM, in *Biogeochemistry of Marine Dissolved Organic Matter*, edited by D. A. Hansell and C. A. Carlson, 2nd ed., pp. 509–533, Academic Press, Boston, doi:10.1016/B978-0-12-405940-5.00011-X.

Retamal, L., W. F. Vincent, C. Martineau, and C. L. Osburn (2007), Comparison of the optical properties of dissolved organic matter in two river-influenced coastal regions of the Canadian Arctic, *Estuarine Coastal Shelf Sci.*, *72*, 261–272, doi:10.1016/j.ecss.2006.10.022.

Retamal, L., S. Bonilla, and W. F. Vincent (2008), Optical gradients and phytoplankton production in the Mackenzie River and the coastal Beaufort Sea, *Polar Biol.*, *31*(3), 363–379.

Romanovsky, V. E., S. L. Smith, and H. H. Christiansen (2010), Permafrost thermal state in the polar Northern Hemisphere during the International Polar Year 2007–2009: A synthesis, *Permafrost Periglac. Process.*, *21*, 106–116, doi:10.1002/ppp.689.

Ruggaber, A., R. Dlugi, and T. Nakajima (1994), Modelling radiation quantities and photolysis frequencies in the troposphere, *J. Atmos. Chem.*, *18*(2), 171–210.

Schröder, D., D. L. Feltham, D. Flocco, and M. Tsamados (2014), September Arctic sea-ice minimum predicted by spring melt-pond fraction, *Nat. Clim. Change*, *4*, 353–357, doi:10.1038/nclimate2203.

Scully, N., and M. W. L. Miller (2000), Spatial and temporal dynamics of colored dissolved organic matter in the north water polynya, *Geophys. Res. Lett.*, *27*, 1009–1011, doi:10.1029/1999GL007002.

Seredynska-Sobecka, B., C. A. Stedmon, R. Boe-Hansen, C. K. Waul, and E. Arvin (2011), Monitoring organic loading to swimming pools by fluorescence excitation-emission matrix with parallel factor analysis (PARAFAC), *Water Res.*, *45*(6), 2306–2314.

Serreze, M. C., M. M. Holland, and J. Stroeve (2007), Perspectives on the Arctic's shrinking sea ice cover, *Science*, *315*, 1533–1536, doi:10.1126/science.1139426.

Shutova, Y., A. Baker, J. Bridgeman, and R. K. Henderson (2014), Spectroscopic characterisation of dissolved organic matter changes in drinking water treatment: From PARAFAC analysis to online monitoring wavelengths, *Water Res.*, *54*, 159–169.
Smith, L. C., T. M. Pavelsky, G. M. MacDonald, A. I. Shiklomanov, and R. B. Lammers (2007), Rising minimum daily flows in northern Eurasian rivers: A growing influence of groundwater in the high-latitude hydrologic cycle, *J. Geophys. Res.*, *112*, G04S47, doi:10.1029/2006JG000327.
Solomon, S., R. W. Portmann, and D. W. J. Thomas (2007), Contrasts between Antarctic and Arctic ozone depletion, *Proc. Natl. Acad. Sci. U.S.A.*, *104*(2), 445–449.
Spencer, R. G. M., G. R. Aiken, K. P. Wickland, R. G. Striegl, and P. J. Hernes (2008), Seasonal and spatial variability in dissolved organic matter quantity and composition from the Yukon River Basin, Alaska, *Global Biogeochem. Cycles*, *22*, GB4002, doi:10.1029/2008GB003231.
Spencer, R. G. M., et al. (2009), Photochemical degradation of dissolved organic matter and dissolved lignin phenols from the Congo River, *J. Geophys. Res.*, *114*, G03010, doi:10.1029/2009JG000968.
Spencer, R. G. M., K. D. Butler, and G. R. Aiken (2012), Dissolved organic carbon and chromophoric dissolved organic matter properties of rivers in the U.S.A., *J. Geophys. Res.*, *117*, G03001, doi:10.1029/2011JG001928.
Stedmon, C. A., and R. Bro (2008), Characterizing dissolved organic matter fluorescence with parallel factor analysis: A tutorial, *Limnol. Oceanogr. Methods*, *6*, 572–579.
Stedmon, C. A., and S. Markager (2001), The optics of chromophoric dissolved organic matter (CDOM) in the Greenland Sea: An algorithm for differentiation between marine and terrestrially derived organic matter, *Limnol. Oceanogr.*, *46*, 2087–2093.
Stedmon, C. A., and S. Markager (2005a), Resolving the variability of dissolved organic matter fluorescence in a temperate estuary and its catchment using PARAFAC analysis, *Limnol. Oceanogr.*, *50*, 686–697.
Stedmon, C. A., and S. Markager (2005b), Tracing the production and degradation of autochthonous fractions of dissolved organic matter using fluorescence analysis, *Limnol. Oceanogr.*, *50*(5), 1415–1426.
Stedmon, C. A., S. Markager, and R. Bro (2003), Tracing dissolved organic matter in aquatic environments using a new approach to fluorescence spectroscopy, *Mar. Chem.*, *82*, 239–254, doi:10.1016/S0304-4203(03)00072-0.
Stedmon, C. A., S. Markager, L. Tranvik, L. Kronberg, T. Slätis, and W. Martinsen (2007a), Photochemical production of ammonium and transformation of dissolved organic matter in the Baltic Sea, *Mar. Chem.*, *104*, 227–240, doi:10.1016/j.marchem.2006.11.005.
Stedmon, C. A., D. N. Thomas, M. Granskog, H. Kaartokallio, S. Papadimitriou, and H. Kuosa (2007b), Characteristics of dissolved organic matter in baltic coastal sea ice: Allochthonous or autochthonous origins?, *Environ. Sci. Technol.*, *41*, 7273–7279.
Stedmon, C. A., R. M. W. Amon, A. J. Rinehart, and S. A. Walker (2011), The supply and characteristics of colored dissolved organic matter (CDOM) in the Arctic Ocean: Pan Arctic trends and differences, *Mar. Chem.*, *124*, 108–118, doi:10.1016/j.marchem.2010.12.007.
Stroeve, J., M. M. Holland, W. Meier, T. Scambos, and M. Serreze (2007), Arctic sea ice decline: Faster than forecast, *Geophys. Res. Lett.*, *34*, L09501, doi:10.1029/2007GL029703.
Stubbins, A., and T. Dittmar (2012), Low volume quantification of dissolved organic carbon and dissolved nitrogen, *Limnol. Oceanogr. Methods*, *10*, 347–352, doi:10.4319/lom.2012.10.347.
Stubbins, A., V. Hubbard, G. Uher, C. S. Law, R. C. Upstill-Goddard, G. R. Aiken, and K. Mopper (2008), Relating carbon monoxide photoproduction to dissolved organic matter functionality, *Environ. Sci. Technol.*, *42*, 3271–3276.
Stubbins, A., R. G. M. Spencer, H. Chen, P. G. Hatcher, K. Mopper, P. J. Hernes, V. L. Mwamba, A. M. Mangangu, J. N. Wabakanghanzi, and J. Six (2010), Illuminated darkness: Molecular signatures of Congo River dissolved organic matter and its photochemical alteration as revealed by ultrahigh precision mass spectrometry, *Limnol. Oceanogr.*, *55*, 1467–1477, doi:10.4319/lo.2010.55.4.1467.
Stubbins, A., J.-F. Lapierre, M. Berggren, Y. Prairie, T. Dittmar, and P. del Giorgio (2014), What's in an EEM? Molecular signatures associated with dissolved organic fluorescence in boreal Canada, *Environ. Sci. Technol.*, *48*(18), 10,598–10,606, doi:10.1021/es502086e.
Tanaka, K., K. Kuma, K. Hamasaki, and Y. Yamashita (2014), Accumulation of humic-like fluorescent dissolved organic matter in the Japan Sea, *Sci. Rep.*, *4*, 5292.
Tranvik, L. J., and S. Bertilsson (2001), Contrasting effects of solar UV radiation on dissolved organic sources for bacterial growth, *Ecol. Lett.*, *4*, 458–463, doi:10.1046/j.1461-0248.2001.00245.x.
Tranvik, L. J., H. Olofsson, and S. Bertilsson (1999), Photochemical effects on bacterial degradation of dissolved organic matter in lake water, in *Microbial Biosystems: New Frontiers Proceedings of the 8th International Symposium on Microbial Ecology*, edited by C. R. Bell, M. Brylinsky, and P. Johnson-Green, Atlantic Canada Society for Microbial Ecology, Halifax, Canada.
Tranvik, L., and S. Kokalj (1998), Decreased biodegrability of algal DOC due to interactive effects of UV radiation and humic matter, *Aquat. Microb. Ecol.*, *14*, 301–307.
Vahatalo, A. V., and R. G. Wetzel (2004), Photochemical and microbial decomposition of chromophoric dissolved organic matter during long (months–years) exposures, *Mar. Chem.*, *89*, 313–326, doi:10.1016/j.marchem.2004.03.010.
Vavrus, S., M. M. Holland, and D. A. Bailey (2010), Changes in Arctic clouds during intervals of rapid sea ice loss, *Clim. Dyn.*, *36*, 1475–1489, doi:10.1007/s00382-010-0816-0.
Walker, S. A., R. M. W. Amon, C. Stedmon, S. Duan, and P. Louchouarn (2009), The use of PARAFAC modeling to trace terrestrial dissolved organic matter and fingerprint water masses in coastal Canadian Arctic surface waters, *J. Geophys. Res.*, *114*, G00F06, doi:10.1029/2009JG000990.
Wang, M., and J. E. Overland (2009), A sea ice free summer Arctic within 30 years?, *Geophys. Res. Lett.*, *36*, L07502, doi:10.1029/2009GL037820.
Wang, X., and J. R. Key (2005), Arctic surface, cloud, and radiation properties based on the AVHRR polar pathfinder dataset. Part II: Recent trends, *J. Clim.*, *18*, 2575–2593.
Williamson, C. E., P. J. Neale, G. Grad, H. J. De Lange, and B. R. Hargreaves (2001), Beneficial and detrimental effects of UV on aquatic organisms: Implications of spectral variation, *Ecol. Appl.*, *11*(6), 1843–1857.
Yamashita, Y., R. M. Cory, J. Nishioka, K. Kuma, E. Tanoue, and R. Jaffé (2010a), Fluorescence characteristics of dissolved organic matter in the deep waters of the Okhotsk Sea and the northwestern North Pacific Ocean, *Deep Sea Res., Part II*, *57*, 1478–1485.
Yamashita, Y., L. J. Scinto, N. Maie, and R. Jaffe (2010b), Dissolved organic matter characteristics across a subtropical wetland landscape: Application of optical properties in the assessment of environmental dynamics, *Ecosystems*, *13*, 1006–1019.
Yamashita, Y., B. D. Kloeppel, J. Knoepp, G. L. Zausen, and R. Jaffe (2011), Effects of watershed history on dissolved organic matter characteristics in headwater streams, *Ecosystems*, *14*, 1110–1122.
Yamashita, Y., J. N. Boyer, and R. Jaffe (2013), Evaluating the distribution of terrestrial dissolved organic matter in a complex coastal ecosystem using fluorescence spectroscopy, *Cont. Shelf Res.*, *66*, 136–144.